Quaternary Science Reviews 331 (2024) 108623

Contents lists available at ScienceDirect

Quaternary Science Reviews

journal homepage: www.elsevier.com/locate/quascirev

New constraints on the Middle-Late Pleistocene Campi Flegrei explosive activity and Mediterranean tephrostratigraphy (~160 ka and 110–90 ka)

Giada Fernandez [a,b,*], Biagio Giaccio [b], Antonio Costa [c], Lorenzo Monaco [b,d], Sébastien Nomade [e], Paul G. Albert [f], Alison Pereira [g], Molly Flynn [f], Niklas Leicher [h], Federico Lucchi [i], Paola Petrosino [j], Danilo M. Palladino [a], Alfonsa Milia [k], Donatella Domenica Insinga [k], Sabine Wulf [l], Rebecca Kearney [m], Daniel Veres [n], Diana Jordanova [o], Maria Luisa Putignano [b], Roberto Isaia [p], Gianluca Sottili [a]

[a] Department of Earth Sciences, "Sapienza" University of Rome, Rome, Italy
[b] Istituto di Geologia Ambientale e Geoingegneria, CNR, Rome, Italy
[c] Istituto Nazionale di Geofisica e Vulcanologia, Sezione di Bologna, Bologna, Italy
[d] CNR-ISMAR, Sede Secondaria di Bologna, Via Piero Gobetti 101, 40129, Bologna, Italy
[e] Laboratoire de Sciences du Climat et de l'Environnement, CEA, UMR 8212, UVSQ, IPSL and Université de Paris-Saclay, Gif-sur-Yvette, France
[f] Department of Geography, Swansea University, Swansea, SA2 8PP, United Kingdom
[g] Université Paris-Saclay, UMR 8148, Laboratoire, GEOPS, Orsay, France
[h] Institute of Geology and Mineralogy, University of Cologne, Cologne, Germany
[i] Dipartimento di Scienze Biologiche, Geologiche e Ambientali, Università di Bologna, 40126, Bologna, Italy
[j] Dipartimento di Scienze della Terra, dell'Ambiente e delle Risorse, Università degli Studi di Napoli Federico II, Naples, Italy
[k] CNR-ISMAR, Istituto di Scienze Marine, Calata Porta di Massa, Interno Porto di Napoli 80, 80133, Napoli, Italy
[l] School of the Environment, Geography and Geosciences, University of Portsmouth, Portsmouth, PO1 3HE, United Kingdom
[m] GFZ German Research Center for Geoscience, Section Climate Dynamics and Landscape Evolution, Telegrafenberg, 14473, Potsdam, Germany
[n] Institute of Speleology, Romanian Academy, Clinicilor 5, 400006, Cluj-Napoca, Romania
[o] National Institute of Geophysics, Geodesy and Geography, Bulgarian Academy of Sciences, Acad. G. Bonchev, bl.3, 1113, Sofia, Bulgaria
[p] Istituto Nazionale di Geofisica e Vulcanologia, Sezione di Napoli Osservatorio Vesuviano, Naples, Italy

ARTICLE INFO

Handling Editor: Dr Giovanni Zanchetta

Keywords:
Tephrochronology
Campi Flegrei
Middle-Late Pleistocene
EMPA and LA-ICP-MS
$^{40}Ar/^{39}Ar$ geochronology
Grain-size

ABSTRACT

The Campi Flegrei (CF) caldera, in southern Italy, is the source of some of the most powerful Late Pleistocene eruptions of the European sub-continent (e.g., Campanian Ignimbrite, Neapolitan Yellow Tuff eruptions). Although the CF caldera has been continuously and intensively investigated for decades, relatively little is known regarding its earliest volcanic activity. In this work, integrating existing and new tephrostratigraphic data, we provide a comprehensive and updated framework for the CF volcanic activity which has occurred at ~160 ka and between ~110 ka and ~90 ka. The new tephrostratigraphic, geochemical (EMPA + LA-ICP-MS), chronological ($^{40}Ar/^{39}Ar$ dating) and grain-size distribution data relate to CF tephra deposits preserved in mid-proximal (Campanian Plain), distal (Tyrrhenian Sea) and ultra-distal (Lower Danube area) sedimentary archives. Our results allowed us to recognize the presence of at least 13 CF eruptions covering the investigated time frame, with 12 eruptions occurring between 110 and 90 ka. Our high-resolution stratigraphic and chronological investigation also allowed us to recognize that the Triflisco/C-22 tephra, previously considered as a single marker layer, can be actually separated into three different events, sourced from within the CF area in the short time interval of ~93-90 ka, suggesting a more complex and intense volcanic history than previously thought. Moreover, a Bayesian age-depth model, constrained by previous and new high precision $^{40}Ar/^{39}Ar$ ages, has led to a reliable estimate of the ages of those undated CF eruptions. Overall, the updated framework on the stratigraphy, chronology, dispersion, and geochemistry of the CF tephra of ~160 ka and between 110 ka and 90 ka consolidates the notion that the Middle-Late Pleistocene activity in theCF area represents a significant stage of its volcanic evolution, characterised by intense and frequent explosive eruptions.

* Corresponding author. Department of Earth Sciences, "Sapienza" University of Rome, Rome, Italy.
E-mail address: giada.fernandez@uniroma1.it (G. Fernandez).

https://doi.org/10.1016/j.quascirev.2024.108623
Received 30 November 2023; Received in revised form 23 February 2024; Accepted 17 March 2024
Available online 5 April 2024

1. Introduction

Detailed reconstructions of the physical (e.g., intensity and magnitude) and temporal (e.g., time-recurrence, temporal clustering) parameters of past explosive volcanism are crucially needed for understanding the processes underlying and leading the Earth's dynamics, which are in turn essential for hazard assessment and risk mitigation purposes (e.g., Sulpizio et al., 2008; Marti et al., 2016; Silleni et al., 2020; Smith et al., 2020; Massaro et al., 2023). Tephra layers recorded in distal successions have long been recognized as powerful integrative tools for reconstructing the eruptive history of past explosive activity (e.g., Lowe, 2011). It is now well demonstrated that near-vent, sub-aerial volcanic successions often provide only fragmentary records of past volcanic activity, due to volcano-tectonic (e.g., caldera-forming events) and sedimentary and surface dynamics processes (e.g., deposition of thick successions, erosion, weathering and/or pedogenesis) they experienced over time (e.g., Albert et al., 2019; Natale et al., 2022a). Indeed, diagnostic stratigraphic, geochemical, and geochronological features of tephra deposits preserved in distal sedimentary archives, characterised by mostly undisturbed deposition of tephra layers and non-volcanic material, can be used to trace the volcanic sources of the tephra, thus providing pivotal information on past explosive activity. Such approach enables to re-assess recurrence times and dynamics of past explosive eruptions at higher temporal resolution and extent (e.g., Albert et al., 2019; Chen et al., 2022; Monaco et al., 2022a), allowing the explosive volcanic history to be traced in a more complete and detailed way.

Neapolitan volcanoes (i.e., Somma-Vesuvius, Campi Flegrei, Procida, and Ischia) produced widespread tephra layers during the Late Quaternary that can be found in several distal records, mostly over the central Mediterranean area (e.g., Sulpizio et al., 2008; Costa et al., 2012; Sulpizio et al., 2012; Satow et al., 2015). Campi Flegrei (CF hereafter), a caldera system located west of the urban area of Naples, is one of the most productive volcanoes of the Mediterranean area (e.g., Di Vito et al., 1999; Smith et al., 2011). Its most recent volcanic history comprises at least two major caldera-forming eruptions: the Campanian Ignimbrite (CI; 39.85 ± 0.12 ka; Giaccio et al., 2017a; Silleni et al., 2020) and the Neapolitan Yellow Tuff (NYT; 14.90 ± 0.40 ka; Deino et al., 2004) that are preserved in proximal to distal locations and, together with smaller eruptions, contributed to the CF current landscape (Vitale and Isaia, 2014; Natale et al., 2022b and references therein). According to alternative interpretations, the Campanian area is characterised, since the Late Pleistocene, by large ignimbrite eruptions which deposits are present onshore and offshore, forming fault-controlled wedges (Milia, 2000; Milia and Torrente, 2007, 2011; Torrente et al., 2010).

In medial and distal tephrostratigraphic records several widespread ash layers have been tentatively linked to poorly constrained activity at CF. One such widespread marker is the Y-3 tephra, which was identified in sediment cores from across the central Mediterranean, and was dated to ~29 ka (e.g., Zanchetta et al., 2008; Vogel et al., 2010; Albert et al., 2015). Recent investigations have unequivocally linked this widespread tephra to CF, and furthermore used largely distal tephrostratigraphic data to reconstruct the volume and dynamics of this large-magnitude eruption (Albert et al., 2019).

This eruption, named Masseria del Monte Tuff (29.3 ± 0.7 ka; Albert et al., 2019), produced up to hundreds of thousands of km^2 of ash covering, with an estimated volume of 16 km^3 DRE (Dense Rock Equivalent) of magma and a Volcanic Explosivity Index (VEI; Newhall and Self, 1982) >6. It constitutes, so far, the third-largest eruption of CF after the NYT and CI eruptions. These recent findings drastically reduce the recurrence times of large-magnitude events at CF, thus having considerable implications for volcanic hazard assessment.

However, while the most powerful Late Pleistocene (e.g., post-NYT

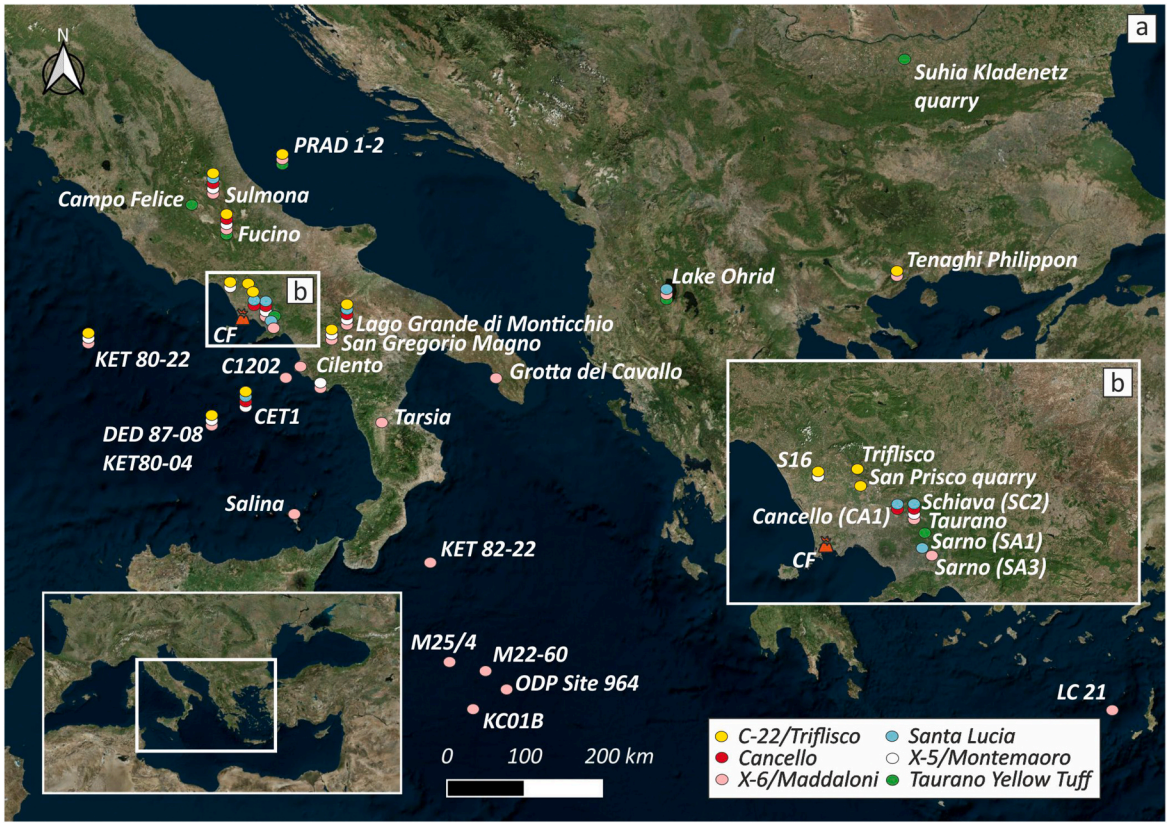

Fig. 1. a) Map of locations where tephra layers ascribed to the ~160 ka and ~110-90 ka volcanic activity of CF were found. CF: Campi Flegrei. b) Map of the Campanian Plain with detailed locations of the tephra layers deposited within the time-interval we considered in this study. A detailed description of the samples' locations and literature sources is provided in Table S1 (Supplementary Material).

and partially post-CI) eruptions at CF have been the subject of extensive investigations (e.g., Di Vito et al., 1999; Smith et al., 2011), only recently the studies on the pre-CI eruptive history (Paterne et al., 1988; Di Vito et al., 2008; Insinga et al., 2014; Monaco et al., 2022a; Tomlinson et al., 2022 and references therein; Vineberg et al., 2023) have been carried out. Specifically, some of the most widespread Middle-Late Pleistocene Mediterranean tephra layers were recently linked to a pre-CI activity that occurred between ~60 ka and 50 ka (e.g., Vineberg et al., 2023) and between ~200 ka and 90 ka (e.g., Wulf et al., 2012; Petrosino et al., 2016; Giaccio et al., 2017b; Monaco et al., 2022a, 2022b), extending back in time the eruptive history of CF.

To provide a comprehensive and updated framework for the CF activity occurred at ~160 ka and between 110 ka and 90 ka, we made a critical literature review and re-assessed the existing datasets of recognized distal CF tephra in the light of new investigations, including major-trace element analysis and $^{40}Ar/^{39}Ar$ dating, carried out on mid-proximal (Campanian Plain), distal (Tyrrhenian Sea) and ultra-distal (Lower Danube area) sedimentary archives (Fig. 1). Moreover, new grain-size data were provided for a large number of previous and newly investigated CF tephra, which is fundamental for future modelling of explosive eruptions.

2. Volcanic activity at Campi Flegrei >90 ka

Since the last decades many tephra layers older than 90 ka with a typical 'Campanian' high-K phono-trachytic geochemical fingerprint, including, among other, the X-6, X-5 and C-22 MIS (Marine Isotope Stage) 5 marker layers, have been documented in the Mediterranean area, both in marine and terrestrial records (e.g., Keller et al., 1978; Paterne et al., 1988, 2008; Munno and Petrosino, 2007; Wulf et al., 2012; Giaccio et al., 2012, 2017b; Bourne et al., 2015; Leicher et al., 2016, 2019, Fig. 1 and Table S1, Supplementary Material). Major element glass compositional data were provided by different authors (e.g., Keller et al., 1978; Sulpizio et al., 2010; Giaccio et al., 2012; Wulf et al., 2012; Donato et al., 2016) as a first step to ascribe them to a generic 'Campanian source'. In addition, some samples were also analysed for trace elements and Sr and Nd isotope compositions, which all highlighted the affinity with CF, therefore the most probable source for these tephra layers (e.g., Insinga et al., 2014; Giaccio et al., 2012, 2017b; Wulf et al., 2012, 2018; Petrosino et al., 2019).

Recently, Monaco et al. (2022a) provided a comprehensive geochemical and geochronological characterization of pumice fallout deposits outcropping in the Campanian Plain spanning the 110-90 ka interval, allowing us to firmly link these pyroclastic units to some of the most widespread MIS 5 Mediterranean marker tephra layers, and to ascribe them to an intense, though still unknown, Campi Flegrei eruptions. Deeper in time, though distal tephra attributions to CF become uncertain, tephra layers with Campi Flegrei geochemical signatures are traced back to ~131 ka in the Lago Grande di Monticchio lacustrine record (i.e., the base of the maar sedimentary succession (Wulf et al., 2012) to ~200 ka in the central Mediterranean marine records (e.g., Paterne et al., 2008) and the Fucino paleolake (Monaco et al., 2022b) while possibly as back as far as ~240 ka in San Gregorio Magno (Petrosino et al., 2019) (Fig. 1).

As far as the evidence in more proximal settings is concerned, De Vivo et al. (2001) and Rolandi et al. (2003) documented an activity in the Campanian area between ~290-160 ka. This Middle Pleistocene activity includes the Seiano (~250 ka), Moschiano (~188 ka) and Taurano (~160 ka) ignimbrites (De Vivo et al., 2001; Rolandi et al., 2003), and other pyroclastic deposits (i.e., Taurano Layered Tuff Series, 207-188 ka; De Vivo et al., 2001; Belkin et al., 2016). The source areas of these deposits are poorly constrained geographically and are thus loosely attributed to the explosive activity in the 'Campanian Volcanic Zone' (De Vivo et al., 2001; Rolandi et al., 2003). Similarly to the 110-90 ka Campanian Plain tephra deposits and distal equivalents (Monaco et al., 2022a), the major and trace element compositions, along with Sr–Nd isotopes of some of these units, point to CF as the most probable source region for these Middle Pleistocene eruptions (e.g., Giaccio et al., 2017b; Petrosino et al., 2019; Monaco et al., 2022b).

So far, among all the Middle Pleistocene medial-distal eruption deposits potentially attributable to CF explosive activity, the Taurano ignimbrite (~160 ka) is currently considered responsible for the most widespread tephra dispersal based on available distal tephrostratigraphic data (e.g., Giaccio et al., 2017b).

3. Materials and methods

3.1. Literature review

In order to provide an updated and comprehensive state of the art of Campi Flegrei (CF) explosive activity older than 90 ka, we focused on the well-investigated interval between ~110 and ~90 ka and on the Taurano Ignimbrite correlatives (~160 ka). Though other tephra potentially sourced in the CF are documented in distal archives for the interval >110 and > 160 ka, we avoided addressing their investigation due to the paucity of data, that prevents a firm and consistent attribution to the CF. With this regard, we collected and summarised all the available literature information on CF tephra layers related, or potentially related, to the CF volcanic activity spanning the ~110-90 ka interval and around 160 ka, recognized from proximal to distal and ultra-distal settings. Specifically, some distal sedimentary archives have been pivotal for tephrochronological purposes, i.e., the Fucino (e.g, Giaccio et al., 2017b) and Sulmona Basins (e.g., Regattieri et al., 2017), the Adriatic (e.g., Bourne et al., 2015), Tyrrhenian (e.g., Paterne et al., 2008; Petrosino et al., 2016; Sammartini et al., 2019) and Ionian Sea (e.g., Insinga et al., 2014; Vakhrameeva et al., 2021), Lago Grande di Monticchio (e.g., Wulf et al., 2004, 2008, 2006, 2012) and Lake Ohrid (e.g., Caron et al., 2010; Leicher et al., 2016), as they are in favourable downwind positions and are valuable records for studying the past explosive activity of the Campanian area. In particular, several sediment cores have been drilled at Lago Grande di Monticchio (southern Italy), due to its strategic position, to reconstruct the eruption history of the volcanoes located in central and southern Italy (e.g., Wulf et al., 2004, 2008, 2012). Hence, it turned out to be one of the most important high-resolution records for tephrochronological studies.

So far six main eruptions, which are the focus of this paper, have been recognized in the interval between ~110 and ~90 ka and around 160 ka (Fig. 1).

- Taurano Yellow Tuff (160.2 ± 2.0 ka, recalculated from De Vivo et al., 2001);
- Maddaloni/X-6 (109.3 ± 1.0 ka, Monaco et al., 2022a);
- Montemaoro/X-5 (105.6 ± 0.5 ka, Petrosino et al., 2016);
- Cancello/TM-24b (102.5 ± 0.8 ka, Monaco et al., 2022a);
- Santa Lucia/TM-24a (101.2 ± 0.8 ka, Monaco et al., 2022a);
- Triflisco/C-22 (91.8 ± 1.2 ka, Monaco et al., 2022a).

The database we created includes all the information on tephra-samples' label, location, thickness, and the analyses performed (e.g., major/trace element, $^{40}Ar/^{39}Ar$ dating and grain-size analyses, when available), as summarised in Table S1 (Supplementary Material). Depending on their availability, several of these tephra layers from the medial and distal sites, which thanks to previous investigations were ascribed to the eruptions considered in this study, were re-sampled for grain-size analysis (Table S2, Supplementary Material).

3.2. Tephra sampling

The literature information is here integrated with the new major and trace element glass compositions, grain-size and $^{40}Ar/^{39}Ar$ data for different mid to distal tephra layers (Table S2, Supplementary Material). These include pumice and ash fallout units in the Campanian Plain

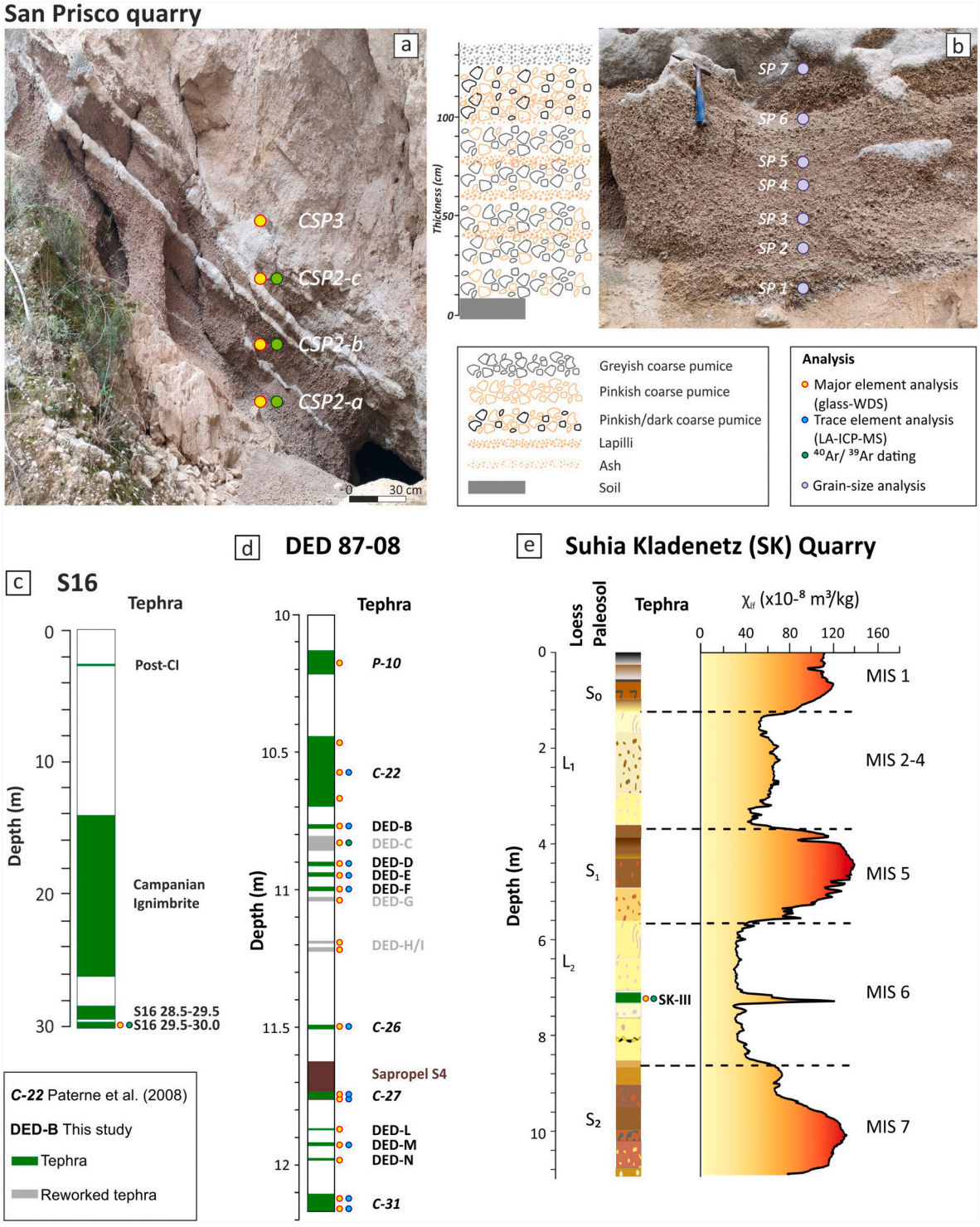

Fig. 2. a) and b) Photographs and stratigraphic log of the San Prisco sequence (41°05′31′′N; 14°17′25′′E, Campanian Plain; Fig. 1). a) CSP2 (a, b and c) and CSP3 were sampled for EMPA and $^{40}Ar/^{39}Ar$ analyses. b) Samples SP1 to SP7 were sampled for grain-size analyses. Full dataset is provided in the Supplementary Material (S1 and S3). c) Simplified section of the core S16 (41°07′02′′N; 14°01′23′′E, Campanian Plain) investigated for the first time in this study; d) Simplified section of the marine core DED 87-08 (39°42′14′′N; 13°34′93′′E, Central Tyrrhenian Sea); e) Loess-paleosol succession of the Suhia Kladenetz Quarry (43°27′24.0″N, 24°41′26.7″E; Central North Bulgaria, Lower Danube). For further details about the core DED 87-08 and Suhia Kladenetz Quarry successions the reader is referred to Paterne et al. (1988, 2008) and Jordanova et al. (2022), respectively.

(units CSP2 and CSP3 from San Prisco quarry; layer 29.5–30.0 in core S16), several tephra layers from the Tyrrhenian Sea marine core DED 87-08 (Paterne et al., 2008) and one tephra (i.e., SK-III) from the Lower Danube loess-paleosol successions (Figs. 1 and 2 and Table S2, Supplementary Material). These sequences and individual samples are described below in detail.

3.2.1. San Prisco quarry (41°05′31′′N; 14°17′25′′E; Campanian Plain)

This succession, outcropping at the eastern margin of the Campanian Plain (Fig. 1), consists of a 110 cm-thick fallout deposit including two

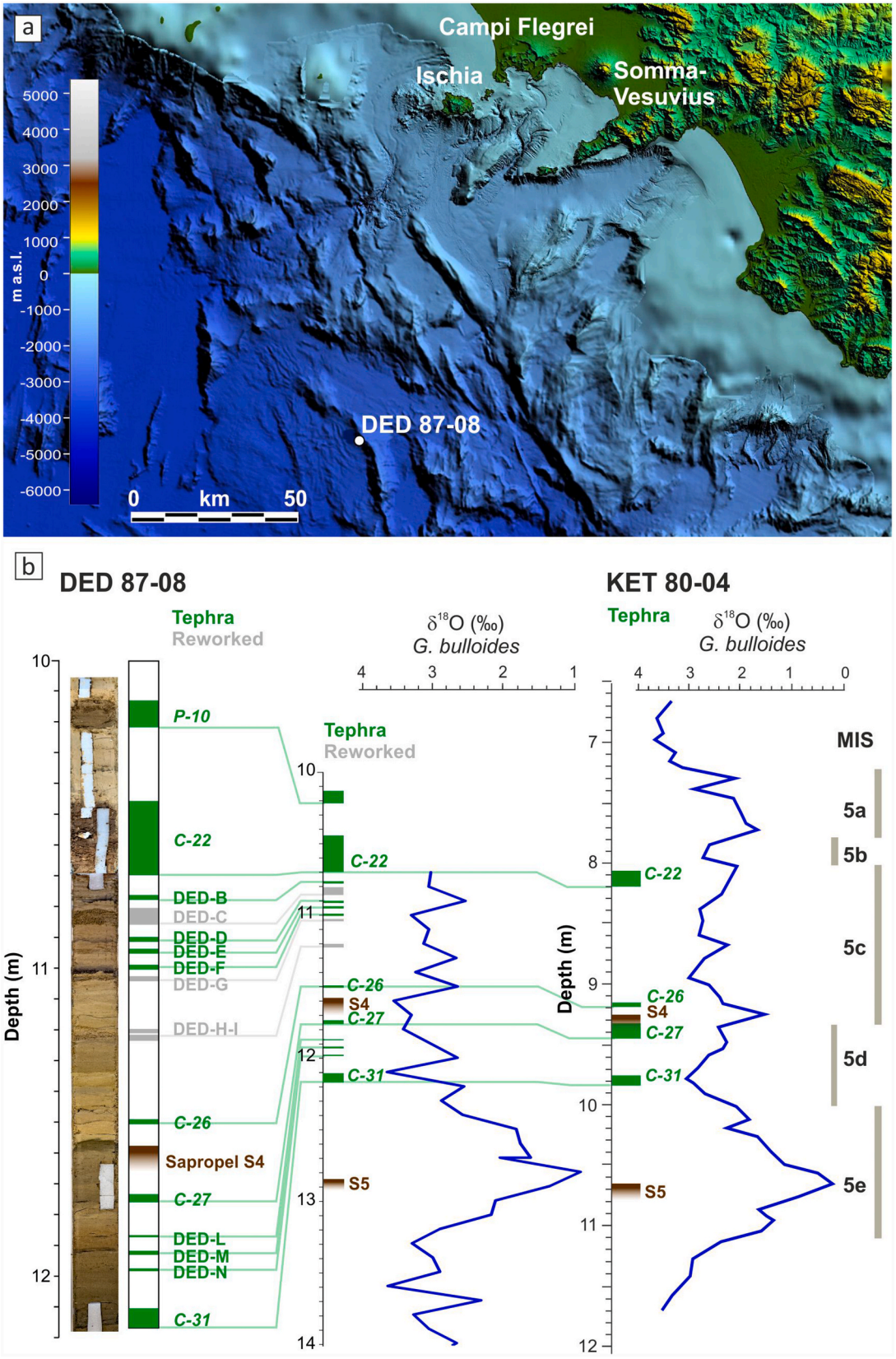

Fig. 3. Reference map and stratigraphy of DED 87-08. a) Digital Terrain Model (DTM) of the eastern Tyrrhenian Sea (Marani and Gamberi, 2004) with location of the DED 87-08 core and of the Neapolitan volcanoes. b) Comparison between DED 87-08 and KET 80-04 MIS 5, tephrostratigraphy, sapropel stratigraphy and oxygen isotope records of *Globigerina bulloides*. For the oxygen isotope records of DED 87-08 and KET 80-04 the reader is referred to Kallel et al. (2000) and Paterne et al. (2008), respectively.

different units, labelled CSP2 and CSP3 (Fig. 2a and b). Overall, eleven samples were collected from this section for major elements, $^{40}Ar/^{39}Ar$ dating and grain-size analyses (Fig. 2a and b).

Specifically, three samples were collected from the CSP2 unit (i.e., CSP2-a, CSP2-b and CSP2-c, see Fig. 2a) for major element analyses and $^{40}Ar/^{39}Ar$ dating, one from the CSP3 unit (i.e., CSP3) for major element glass analysis (Fig. 2a) and seven samples were collected from the CSP2 unit for grain-size analysis (SP1 to SP7, Fig. 2b).

3.2.2. S16 (41°07′02′′N; 14°01′23′′E; Campanian Plain)

The sediment core S16 (Campanian Plain, Fig. 1) was recovered within the project for the Italian Geological Map (CARG-Project; geological sheet 429 - Caserta Ovest). It consists of a ~30 m-thick succession of alluvial-fluvial deposits with intercalation of pyroclastic deposits. The thickest one (~12 m-thick), located between 14 and 26 m depth, has been attributed to the CI (Fig. 2c). Two tephra layers occur below the CI in core S16, at 28.5–29.5 m and 29.5–30.0 m depth, respectively (Fig. 2c). The deepest, 50 cm-thick tephra at 29.5–30.0 m depth in S16 was collected for major element, $^{40}Ar/^{39}Ar$ dating and grain-size analysis.

3.2.3. DED 87-08 (39°42′14′′N; 13°34′93′′E; central Tyrrhenian Sea)

The marine core DED 87-08 has a length of 30.73 m and was collected during the DEDALE-87 cruise at a water depth of 2965 m (Paterne et al., 2008). While the age of the core bottom is not well constrained, oxygen stable isotopes, as well as previous tephrostratigraphic analyses, indicate that the upper ~18 m of the core span the last 200 kyr (Paterne et al., 1988, 2008). Specifically, according to the available oxygen isotope and sapropel stratigraphy, the investigated interval, from 10.13 to 12.08 m in DED 87-08, should span the MIS 5d-MIS 5a interval or ~110-85 ka (Fig. 3; Paterne et al., 2008). Here, 15 visible and stratigraphically discrete layers were sampled for major/-trace element analysis and $^{40}Ar/^{39}Ar$ dating, as detailed in Fig. 2d. These included the previously analysed layers P-10, C-22, C-26, C-27, and C-31, for which Paterne et al. (2008) provided average SEM-EDS data, along with eleven new layers, here labelled 'DED' followed by progressive letters (B to N from top to bottom; Fig. 3). Thick tephra layers (i.e., C-22, C-27 and C-31) were sub-sampled to check for possible chemical variabilities across the layer (Fig. 2d). The thickest tephra layer C-22 (24 cm) was sampled twice, first as a single sample and secondly as three sub-samples (i.e., bottom, middle and top).

3.2.4. Suhia Kladenetz (SK) quarry (43°27′24.0″N, 24°41′26.7″E; central North Bulgaria)

This study site is a 27 m-thick loess-paleosol sequence, including 7 loess units and 6 paleosol complexes, within the Suhia Kladenetz (SK) quarry (Lower Danube loess area; Fig. 1). This succession, spanning the MIS 19-MIS 1 interval (last 800 ka), contains four tephra layers ascribed to the MIS 6 (loess L2), MIS 10 (loess L4), MIS 13 (top paleosol S5) and MIS 15 (base paleosol S5) (Jordanova et al., 2022). Here we analysed the visible tephra layer occurring in MIS 6 loess unit L2 (7.14–7.32 m depth; Fig. 2e). It is a 20 cm-thick light brown tephra layer, made up of both rounded and elongated pumices (max φ 2 mm) and coarse and fine ash. One sample has been collected (labelled SK-III) for major element composition and grain-size analysis (Fig. 2e).

3.3. EMPA-WDS analysis

Major element glass analyses were carried out at the Istituto di Geoscienze e Georisorse of the Italian National Research Council (IGG-CNR; Florence, Italy), with a JEOL Superprobe JXA-8230 equipped with five-WDS (Wavelength Dispersive Spectrometers). Operating conditions were set to 15 kV accelerating voltage, 10 nA beam current and 10 μm defocused beam diameter to limit Na mobilisation. Element counting times were 15 s for all elements except for Na (10 s), F (20 s), S (30 s), Mn, P and Cl (40 s). Albite (Si and Na), ilmenite (Ti and Fe), plagioclase (Al), bustamite (Mn), olivine (Mg), diopside (Ca), sanidine (K), apatite (P), fluorite (F), tugtupite (Cl) and celestine (S) were used as internal standards. The accuracy of the measurements was assessed using the glass secondary standards GOR128-G, ATHO-G and StHs6/80-G (Jochum et al., 2006), Lipari ID3506 (Kuehn et al., 2011), Scapolite NMNH and CFA47 (Marianelli and Sbrana, 1998). All compositional data are shown as oxide weight percentages (wt%) in the *Total alkali vs Silica* (TAS, Le Maitre et al., 2002) and bi-plots diagrams, with total iron measured as FeO and oxide data normalised to 100% on a volatile-free basis for correlation purposes. All collected data are reported in the Supplementary Material S1.

3.4. LA-ICP-MS analysis

Trace element analysis of volcanic glass shards was performed using an Agilent 8900 triple quadrupole ICP-MS (ICP QQQ) coupled to a Resonetics 193 nm ArF excimer laser-ablation in the Department of Earth Sciences, Royal Holloway, University of London (Egham Hill, Egham, UK). Full analytical procedures used are reported in Tomlinson et al. (2010). Spot sizes of 20 and 25 μm were used depending on the vesicularity, crystal content and ultimately the size of available glass surfaces. The repetition rate was 5 Hz, with a count time of 40 s on the sample, and 40 s on the gas blank to allow the subtraction of the background signal. Blocks of eight or nine glass shards and one MPI-DING reference glass were bracketed by the NIST612 glass calibration standard (GeoREM 11/2006). In addition, MPI-DING reference glasses were used to monitor analytical accuracy (Jochum et al., 2005). The internal standard applied was ^{29}Si (determined by EMP-WDS analysis). LA-ICP-MS data reduction was performed in Microsoft Excel®. Accuracies of LA-ICP-MS analyses of MPI-DING glass standards ATHO-G and StHs6/80-G were typically ≤5%. Full glass datasets and MPI-DING standard glass analyses are provided in Supplemental Material. Similarity Coefficient index (SC; Sarna-Wojcicki et al., 1987) and statistical distance (D_2; Perkins et al., 1995) were used to assess the potential correlations. The SC is calculated as the average of ratios of elemental concentrations between pairs of compositional analyses of tephra (calculated as averages). Two samples are considered correlatives if they have an SC value close to 1, with SC > 0.92 considered a lower bounding value for a good statistical correlation. By contrast, statistical distance (D_2) measures the difference between two tephra based on their average compositions and standard deviations. D_2 is a distance function, thus the lower its value the higher the similarity between two samples being compared. Compositionally identical samples have $D_2 = 0$. The use of these SC and D_2 indices is not without problems but in general, the indices are widely used and give a broad numerical-strength indication of the compositional similarity between the two samples. Data averages are reported with a ±2 standard deviation (2 s.d.). Full dataset is provided in the Supplementary Material S1.

3.5. $^{40}Ar/^{39}Ar$ dating

The $^{40}Ar/^{39}Ar$ ages for tephra DED-C (DED 87-08, section X), S16-29.5-30.0, CSP2-a, b, c and CET1 10–14 were obtained at the Laboratoire des Sciences du Climat et de l'Environnement (CEA, CNRS UMR 8212, Gif-sur-Yvette, France) dating facility. Between 40 and 100 fresh and transparent K-rich feldspars were picked for each sample. After being washed in distilled water, transparent K-feldspars (350–500 μm) without visible inclusions were handpicked under a binocular and used for dating. Beforehand, irradiated crystals were leached for 5 min in a 10% HF solution to remove potential groundmass pieces and alteration phases that could be still attached at the surface of the crystals. Twenty to thirty crystals for each sample were irradiated in the Cd-lined, in the core CLICIT facility of the Oregon State University TRIGA reactor for 1 h in two distinct irradiations, IRR. CO-016, (Level C) and IRR. CO19 (S16-29.5-30.0, CSP2-a, b, c and CET1 10–14). Interference corrections were based on the nucleogenic production ratios given in Balbas et al. (2016).

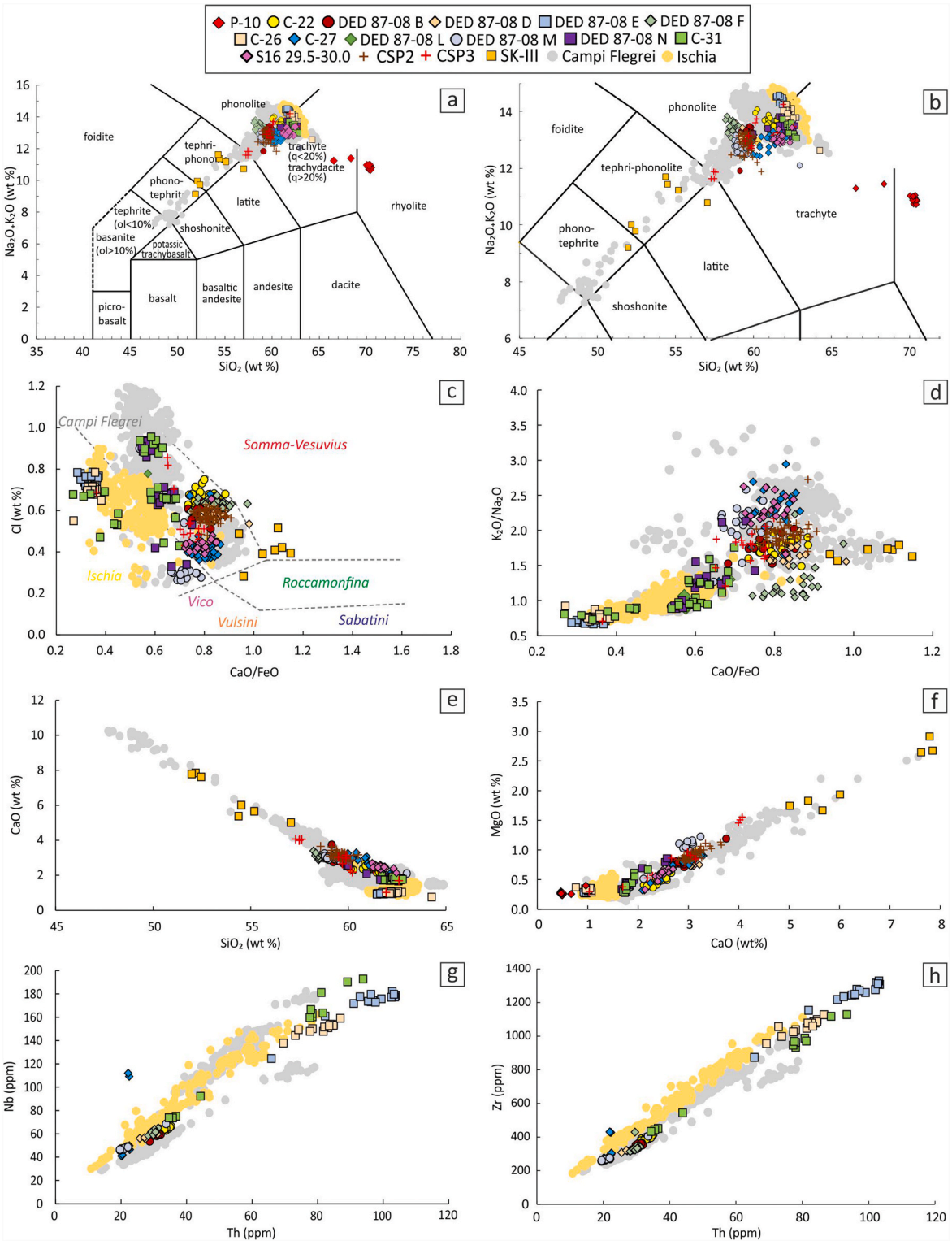

Fig. 4. Major element composition of the samples from marine core DED 87-08, S16 core, San Prisco Quarry and Suhia Kladenetz (SK) Quarry, in comparison with literature data of Campi Flegrei and Ischia samples. **a)** and **b)** Total alkali vs silica (TAS, Le Maitre et al., 2002); **c)** CaO/FeO vs Cl diagram (modified after Giaccio et al., 2017b); **d)** CaO/FeO vs K_2O/Na_2O; **e)** SiO_2 vs CaO; **f)** CaO vs Mg; **g)** Th vs Nb; **h)** Th vs Zr. Major and trace element data source: P-10 to C-31, S16 29.5–30.0, CSP2, CSP3 and SK-III: this study; Campi Flegrei (grey dots): Tomlinson et al. (2012), Vineberg et al. (2023); Ischia (yellow dots): Tomlinson et al. (2014), Vineberg et al. (2023). More detailed data on major element composition can be found in the Supplementary Material S1.

After irradiation, crystals were transferred into a copper 133 pits sample holder placed into a differential vacuum Teledyne Cetac window connected to a home-designed compact extraction line. Minerals were fused one by one using a 100 W Teledyne Cetac CO_2 laser during 15 s at 2.5 W. Before fusion, each crystal underwent a 20 s long sweeping at 0.3 W to remove unwanted gas potentially trapped on the crystals surface and fractures. Extracted gases were firstly purified by a SAES GP 50 cold getter for 90 s and then for 230 s by two hot SAES GP 50 getters. The five

Argon isotopes (i.e., ^{40}Ar, ^{39}Ar, ^{38}Ar, ^{37}Ar and ^{36}Ar) were measured using a multi-collector NGX 600 mass spectrometer equipped with 9 ATONA® amplifiers array and an electron multiplier. More technical specifications regarding the NGX 600 ATONA detector array are presented in detail in Cox et al. (2020). ^{40}Ar, ^{39}Ar, ^{38}Ar, and ^{36}Ar isotopes were collected simultaneously while the ^{37}Ar was measured in a second time. In the first run, ^{40}Ar, ^{39}Ar and ^{38}Ar were measured simultaneously on 3 ATONA® amplifiers and ^{36}Ar on the electron multiplier. Following this first run, the ^{37}Ar was measured alone using the electron multiplier. Each isotope measurement corresponds to 15 cycles of 20-s integration time. Peak intensity data were reduced using ArArCALC V2.4 (Koppers, 2002). Neutron fluence J factor was calculated using co-irradiated Alder Creek sanidine standard ACs-2, constrained to an age of 1.1891 Ma (Niespolo et al., 2017) according to the K total decay constant of Renne et al. (2011) ($\lambda_{e.c.} = (0.5757 \pm 0.016) \times 10- 10\ yr^{-1}$ and $\lambda\beta^{-} = (4.9548 \pm 0.013) \times 10- 10\ yr^{-1}$)). To determine this neutron flux we used 14 flux monitor crystals coming from pits framing the samples in each irradiation disk. J-values measured are 0.00027330 ± 0.00000011 for Level C; 0.00028400 ± 0.00000017 for S16-29.5-30.0, CSP2-a, b, c and CET1 10–14, which were irradiated at the same level. To verify the detector's linearity, mass discrimination was monitored by analysis of at least 10 air shots of various beam sizes ranging from 1.0 10^{-2} up to 5.0 10^{-2} V (1–5 air shots). About 15 air shots analyses are performed every day. These measurements are done automatically during the nights before and after the unknown measurements. Discrimination is calculated according to the $^{40}Ar/^{36}Ar$ ratio of 298.56 (Lee et al., 2006). Procedural blank measurements were achieved after every two to three unknowns. For a typical 5 min time, blank backgrounds are between 0.6 and 2.3 10^{-4} V for ^{40}Ar and 20–50 cps for ^{36}Ar (about 3.0^{-7} 10^{-7} V equivalent). Full analytical data for each sample can be found in Supplementary Material S2.

3.6. Bayesian age-depth model

Age-depth modelling was performed using the software package Bacon v. 3.2 (Blaauw and Christen, 2011) within the open-source statistical environment R (PsyTeachR Team, 2022). For this purpose, we used the MIS 5 section of the Lago Grande di Monticchio tephra record (Wulf et al., 2012), which is the most complete, high-resolution distal tephrostratigraphy that documents correlatives of investigated tephra in this study. The model comprises the interval between the depths of 57.51 m and 76.00 m of Monticchio composite section, corresponding to the temporal interval of ~89–109 ka, using the MON14 varve chronology published by Wulf et al. (2012) and Martin-Puertas et al. (2014). By assuming an instantaneous deposition of the tephra layers, this depth interval was then converted in the equivalent tephra-free depth interval of 57.51–76.00 m, i.e., the depth net of the thickness of the tephra, which we used for the age-depth model.

For the age input, we used the updated $^{40}Ar/^{39}Ar$ geochronology of six eruptions occurred in the time interval between ~110 and 90 ka, including both published (e.g., Cancello, Santa Lucia and Maddaloni: Monaco et al., 2022a) and the new ages provided in this study for C-22, Triflisco and Montemaoro (i.e., CET1 10–14, CSP-2, S16 29.5–30.0; see details in Sections 3.5 and 4.3). All $^{40}Ar/^{39}Ar$ were recalculated using the software ArAR with a given decay constant of Renne et al. (2011) and an age for ACs-2 at 1.1891 Ma (Niespolo et al., 2017). The modelled interval of the succession was set into 5 cm vertical sections for modelling individual accumulation rates at a 95% confidence interval, which provides the basis for the age-depth model.

3.7. Grain-size analyses

Reliable tephra correlations, grain-size and thickness data are essential when trying to model and reconstruct the eruptive parameters of past explosive eruptions. Grain-size analyses were performed on samples from mid-distal (i.e., Campanian Plain) and distal (i.e., Fucino and Sulmona basin, Tyrrhenian and Ionian Seas, Lago Grande di Monticchio and Lake Ohrid, Danube loess area) locations (Table S1, Supplementary Material). Bulk samples were investigated, to be representative of the total grain-size distribution. Most of the analyses were performed at the Department of Earth Sciences of "Sapienza'' University of Rome (Rome, Italy). The samples were washed with 25-vol H_2O_2 to remove organic matter. The samples were stirred for 3 h in a solution of distilled water and $(NaPO_3)_6$ to break the aggregates and then sieved with a mesh size of 63 μm to separate the coarse (>63 μm) and the fine (<63 μm) fractions. The former was analysed through dry sieving, using a stack of sieves with decreasing meshes from 2 mm to 63 μm. The latter, instead, was analysed through a Sympatec Helos LA S/N 400 laser diffractometer. Analyses of tephra from Lake Ohrid were carried out at the University of Cologne (Cologne, Germany). In this case, untreated material was dispersed using $Na_4P_2O_7$, put on a shaker for 1 h and the analysis performed using a Beckmann Coulter LS 13 320 XR particle analyser. Statistical parameters of each sample were obtained using the GRADISTAT program (Blott and Pye, 2001): i) "mean" (M_z), defined as the average grain-size; ii) "sorting" (σ), that describes the grain-size variation; iii) "skewness", which shows the degree to which the cumulative curve approaches symmetry and iv) "kurtosis", a measure of the sharpness of the peak of a frequency-distribution curve (Folk, 1966). The full dataset is provided in the Supplementary Material S3.

4. Results

4.1. Tephra stratigraphy and glass chemical composition

4.1.1. San Prisco quarry (Campanian Plain)

CSP2 - This unit consists of a ~110 cm-thick pumice fallout deposit laying on pedogenized reworked ash and clastic sediments (Fig. 2a). The lowermost 15 cm-thick layer is made of pinkish/greyish vesicular pumices and ash and contains limestone clasts (Fig. 2a). The following 45 cm-thick layer consists of normal graded, havana-grey pumices (max φ 3 cm) up to fine lapilli (max φ 4 mm). On top, a layer of pinkish pumices shows an inverse grading from ~mm-scale to up to 3–4 cm, with one layer of grey pumiceous lapilli and dark pumices above. The following 25 cm-thick layer is made up of massive, aphyric coarse grey pumices (φ = 3–4 cm). The unit ends up with an inversely graded layer of pinkish coarse ash up to 3 cm-large dark lapilli clasts.

Overall, these lithological features (i.e., colour, pumices shape, vesicularity, and crystals) are the same as described for the Triflisco tephra (Monaco et al., 2022a), thus CSP2 unit represents a new occurrence of the Triflisco Plinian fall from the Campi Flegrei. Its chemical composition (samples CSP2-a, b and c) spans the range between the phonolitic and trachytic fields, with a mean SiO_2 content of 59.64 ± 0.62 wt% and alkali sums of 12.90 ± 0.55 wt% (Fig. 4a and b). CaO/FeO ratios are <1 (0.82 ± 0.07; Fig. 4c), showing a mean Cl content of 0.57 ± 0.06 wt%, and a mean K_2O/Na_2O ratio of 1.95 ± 0.30. All three sub-samples of CSP2 (a, b, c) display the same chemical composition and are hence plotted as a single sample (labelled CSP2) in bivariate diagrams (Fig. 4).

CSP3 - The second sub-unit (i.e., CSP3, see Fig. 2a) overlays the CSP2 and consists of a layer of white coarse and fine ashes. CSP3 glass displays a heterogeneous phonolitic/trachytic composition (Fig. 4a and b), with SiO_2 contents between 57.31 and 62.60 wt% and alkali sums between 11.64 and 14.27 wt%. CaO/FeO values are <1 (0.71 ± 0.20; Fig. 4c) and Cl content of 0.55 ± 0.27 wt%, whilst the mean K_2O/Na_2O ratio is 1.69 ± 0.70.

4.1.2. S16 core (Campanian Plain)

S16 29.5-30.0 m – The unit consists of a greyish, fine-lapilli and ash-rich tephra layer that is trachytic in glass composition (Fig. 4a and b), having a mean SiO_2 content of 61.73 ± 0.61 wt% and alkali sum of 13.06 ± 0.30 wt%. CaO/FeO values are <1 (0.79 ± 0.08; Fig. 4c) and Cl

content is 0.44 ± 0.11 wt%, whilst the mean K_2O/Na_2O ratio is 2.29 ± 0.44.

4.1.3. DED 87-08 core (Tyrrhenian Sea)

Based on the main lithostratigraphic and geochemical features, the fifteen investigated levels from Tyrrhenian Sea core DED 87-08, were classified as 'primary' tephra and 'reworked' layers. In particular, 'primary' tephra layers occur as discrete layers, distinct from each other both in terms of textural and lithological features and geochemical composition. They are characterised by a tabular or lenticular geometry, with a quite well-defined lower and upper boundaries and are made up of 100% glass shards in addition to a few crystals, with a homogenous chemical glass composition that differs from each other. In contrast, the 'reworked' layers appear coarser and fine-depleted, lithologically and geochemically heterogeneous (e.g., multiple volcanic sources based on volcanic glass chemistry) and, above all, contain coarse shell fragments of shallow water organisms.

4.1.3.1. Primary tephra layers in DED 87-08. **P-10** (10.13–10.21 m depth) is an 8 cm-thick dark-grey layer, peralkaline-rhyolite in composition (comendite-like; Fig. 4a and b), showing a SiO_2 content of 69.90 ± 2.20 wt% and Na_2O of 6.20 ± 0.50 wt%. CaO/FeO values are <1 (0.11 ± 0.06) and Cl content is 0.6 ± 0.2 wt%. The sample displays an average FeO content of 4.95 ± 0.26 wt%, Al_2O_3 is 12.59 ± 1.56 wt% and K_2O/Na_2O is 0.77 ± 0.09 (Supplementary Material S1).

C-22 (10.43–10.67 m), the thickest layers in DED 87-08 (24 cm), appears light brown to ochre in colour. Its composition is homogeneous and falls in the range between trachyte and phonolite fields (Fig. 4a and b) with CaO/FeO ratio values < 1 (0.81 ± 0.09), mean Cl content of 0.66 ± 0.08 wt% and K_2O/Na_2O of 1.73 ± 0.30. C-22 is rather homogeneous in terms of incompatible trace element composition (Th = 33 ± 2.52 ppm, Nb = 64.94 ± 2.63 ppm, Zr = 374.05 ± 26.68 ppm, Fig. 4g and h). The ratios of the other High Field Strength Elements (HFSE) to Th are constant (Zr/Th = 11.34 ± 0.47, Nb/Th = 1.97 ± 0.10) and the Light Rare Earth Elements (LREE) are enriched compared to the Heavy Rare Earth Elements (HREE), with La/Yb = 25.77 ± 4.90.

DED-B layer (10.74–10.75 m) is a thin (1 cm) dark grey layer, and it is homogeneous, phonolitic/trachytic in composition (Fig. 4a and b). CaO/FeO values are <1 (0.78 ± 0.09) and Cl content is 0.57 ± 0.11 wt %, with a K_2O/Na_2O ratio of 1.77 ± 0.33. DED-B is homogeneous in terms of incompatible trace element composition (Th = 30.61 ± 1.87 ppm, Nb = 59.55 ± 3.49 ppm, Zr = 332.50 ± 21.80 ppm, Fig. 4g and h). The ratios of the other HFSE to Th is constant (Zr/Th = 10.86 ± 0.39, Nb/Th = 1.95 ± 0.08) and the LREE are enriched compared to the HREE, with La/Yb = 28.21 ± 4.02.

DED-D layer (10.87–10.88 m) is a thin (1 cm) grey layer displaying a homogeneous phonolitic composition (SiO_2 content of 59.70 ± 0.53 wt % and alkali sum of 13.17 ± 0.82 wt%; Fig. 4a and b). CaO/FeO values are <1 (0.84 ± 0.10) and Cl content is 0.57 ± 0.04 wt%, with a K_2O/Na_2O of 1.65 ± 0.26. DED-D is homogeneous in terms of incompatible trace element composition (Th = 27.76 ± 6.08 ppm, Nb = 57.79 ± 6.99 ppm, Zr = 304.62 ± 37.62 ppm, Fig. 4g and h). The ratios of the other HFSE to Th are relatively constant (Zr/Th = 11.03 ± 1.30, Nb/Th = 2.08 ± 0.24) and the LREE are enriched compared to the HREE, with La/Yb = 29.68 ± 4.60.

DED-E (10.90–10.91 m) is a thin (1 cm) light brown tephra. It shows a phonolitic composition (Fig. 4a and b) with a mean SiO_2 content of 61.74 ± 0.37 wt% and alkali sums of 14.42 ± 0.24 wt%. CaO/FeO ratio values are <1 (0.33 ± 0.06) and Cl content is 0.75 ± 0.05 wt%, with a K_2O/Na_2O of 0.69 ± 0.05. DED-E is quite heterogeneous and shows high values of incompatible trace elements (Th = 95.49 ± 20.12 ppm, Nb = 174.64 ± 28.49 ppm, Zr = 1237.68 ± 225.13 ppm, Fig. 4g and h). The ratios of the other HFSE to Th is constant (Zr/Th = 12.99 ± 0.76, Nb/Th = 1.83 ± 0.16) and the LREE are enriched compared to the HREE, with La/Yb = 21.22 ± 1.81.

DED-F (10.95–10.97 m) is a ~2 cm-thick, dark grey tephra showing a predominant phonolitic composition (Fig. 4a and b) displaying SiO_2 contents of 58.66 ± 0.57 wt% and alkali sums of 13.40 ± 0.63 wt%. CaO/FeO ratios are <1 (0.85 ± 0.11) and Cl content is 0.63 ± 0.04 wt% with K_2O/Na_2O of 1.26 ± 0.57. DED-F is homogeneous in terms of incompatible trace element composition (Th = 29.58 ± 1.65 ppm, Nb = 62.68 ± 4.01 ppm, Zr = 318.78 ± 63.45 ppm, Fig. 4g and h). The ratios of the other HFSE to Th is fairly constant (Zr/Th = 10.78 ± 2.15, Nb/Th = 2.12 ± 0.09) and the LREE are enriched compared to the HREE, with La/Yb = 28.90 ± 3.65.

C-26 (11.44–11.45 m) is ochre in colour and only 0.5 cm in thickness. It displays a homogeneous trachytic/phonolitic composition, with a mean SiO_2 content of 62.38 ± 0.96 wt% and an alkali sum of 13.92 ± 0.67 wt% (Fig. 4a and b). CaO/FeO ratios are <1 (0.34 ± 0.05), Cl content is 0.69 ± 0.09 wt%, and mean K_2O/Na_2O ratios are 0.76 ± 0.10. C-26 is homogeneous and rich in incompatible trace elements (Th = 80.64 ± 10.47 ppm, Nb = 152.69 ± 10.27 ppm, Zr = 1053.63 ± 89.35 ppm, Fig. 4g and h). The ratios of the other HFSE to Th is constant (Zr/Th = 13.09 ± 0.93, Nb/Th = 1.89 ± 0.15) and the LREE are enriched compared to the HREE, with La/Yb = 21.58 ± 0.84.

C-27 (11.66–11.69 m) is 3 cm-thick, mostly brown, and trachytic in composition (Fig. 4a and b), with a mean SiO_2 content of 61.14 ± 1.34 wt% and alkali sum of 12.98 ± 0.57 wt%. The sample shows a High Alkali Ratio (HAR) of 2.28 ± 0.67 with CaO/FeO values < 1 (0.79 ± 0.09), a Cl content of 0.43 ± 0.19 wt% and K_2O/Na_2O ratio of 2.28 ± 0.67. C-27 sample is quite heterogeneous in terms of incompatible trace element composition (Th = 21.11 ± 2.34 ppm, Nb = 63.54 ± 66.73 ppm, Zr = 305.62 ± 145.90 ppm, Fig. 4g and h). The ratios of the other HFSE to Th are not constant (Zr/Th = 14.41 ± 5.93, Nb/Th = 3.01 ± 2.94) and the LREE are enriched compared to the HREE, with La/Yb = 29.31 ± 8.66.

DED-L (~11.79 m) is light brown in colour and appears as a very thin and lenticular layer, thus preventing us from finding a large number of glass shards to analyse. However, the shards we were able to analyse display a homogeneous composition, with SiO_2 content of 62.04 ± 0.55 wt% and alkali sum of 13.51 ± 0.28 wt%, thus showing a trachytic composition (Fig. 4a and b). Mean CaO/FeO values are <1 (0.60 ± 0.09) and Cl content is 0.84 ± 0.24 wt%. The mean K_2O/Na_2O ratio is 1.03 ± 0.33.

DED-M (11.84–11.85 m) is 1 cm thick and appears light brown in colour. It shows a mean SiO_2 content of 59.65 ± 2.55 wt% and an alkali sum of 12.74 ± 0.61 wt%, ranging between the trachyte and phonolite fields (Fig. 4a and b). CaO/FeO ratio values are <1 (0.70 ± 0.11) and Cl content is 0.35 ± 0.34 wt%, with a K_2O/Na_2O ratio of 2.01 ± 0.79. DED-M is fairly homogeneous in terms of incompatible trace element composition (Th = 21.51 ± 8.13 ppm, Nb = 49.88 ± 13.10 ppm, Zr = 256.60 ± 86.83 ppm, Fig. 4g and h). The ratios of the other HFSE to Th are constant (Zr/Th = 11.97 ± 0.69, Nb/Th = 2.32 ± 0.22 and the LREE are enriched compared to the HREE, with La/Yb = 28.44 ± 4.69.

DED-N (~11.89 m) appears as a thin light brown and lenticular layer and, as for the DED-L, we were not able to find a significant number of glass shards. However, it displays a homogenous composition with SiO_2 content of 61.89 ± 1.61 wt% and alkali sums of 13.39 ± 0.38 wt%, thus showing a trachytic/phonolitic composition in the Total Alkali vs Silica diagram (Fig. 4a and b). CaO/FeO ratio values are <1 (0.62 ± 0.11) and Cl content is 0.68 ± 0.38 wt%, with a mean K_2O/Na_2O ratio of 1.27 ± 0.71. Trace elements were not analysed for the DED-N sample, either because it was glass-poor or glass shards were too small.

C-31 (12.02–12.08 m) is ~6 cm thick and was analysed in two subsamples, basal (12.08-12-04 m depth) and top (12.04–12.02 m depth). The glass from the basal sample shows a quite homogenous trachytic composition, showing SiO_2 content of 62.75 ± 1.97 wt% and an alkali sum of 13.42 ± 0.65 wt% (Fig. 4a and b). CaO/FeO values are <1 (0.55 ± 0.24) and Cl content is 0.71 ± 0.33 wt%, whilst the K_2O/Na_2O ratio is 1.07 ± 0.53. The sample C-31 top shows instead two distinct glass geochemical compositions, one matching that of the basal

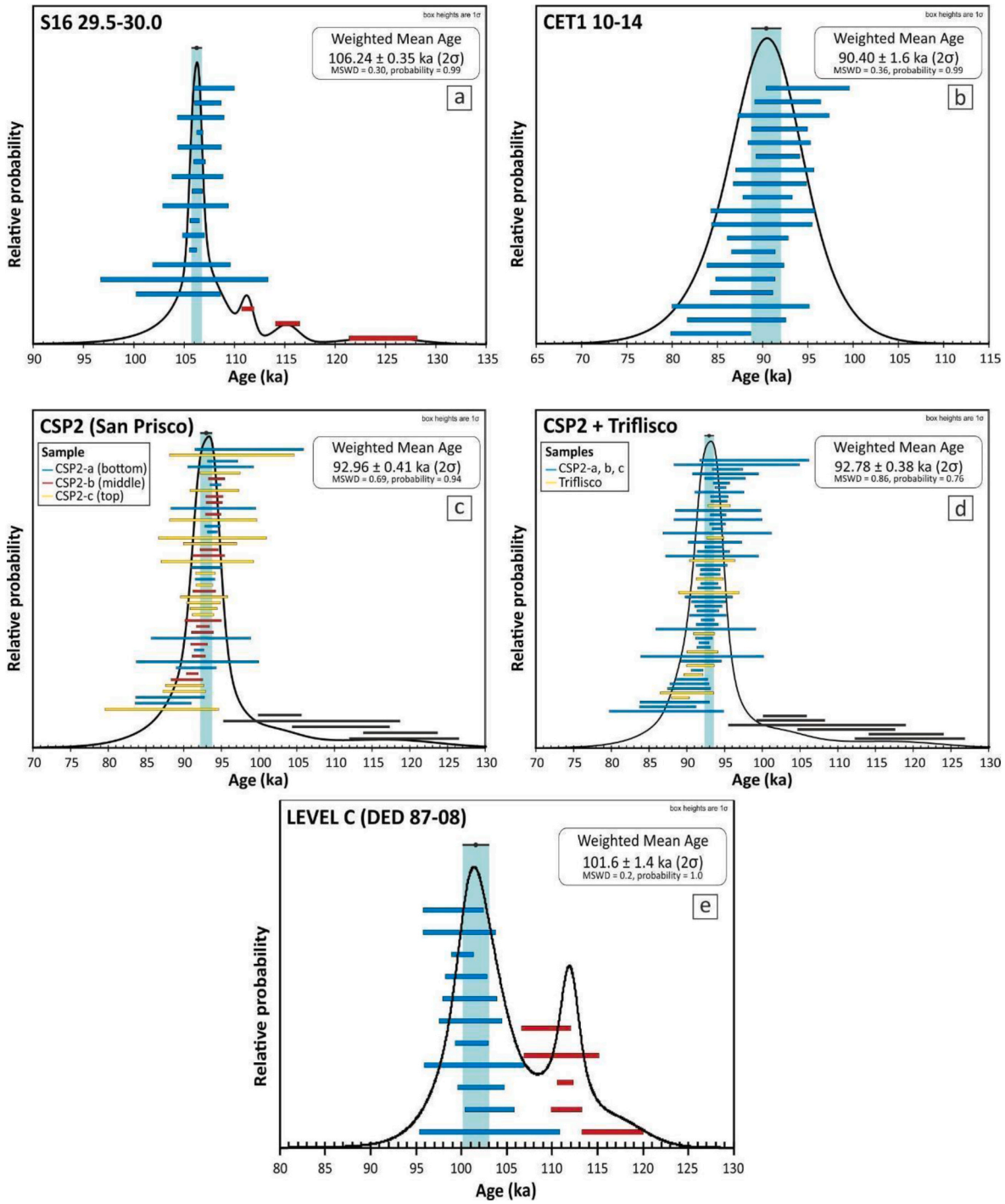

Fig. 5. $^{40}Ar/^{39}Ar$ age probability diagrams for the layers a) S16 29.5–30.0; b) CET1 10–14; c) and d) CSP2-a, b, c and CSP2-a, b, c combined with the age calculated for the Triflisco type locality tephra (Monaco et al., 2022a); e) DED-C (DED 87-08).

sample while the second differing from the first for its very low alkali ratio (<1) and CaO content, ranging from 1.2 to 0.8 (see Supplementary Material S1). C-31 is heterogeneous in terms of incompatible trace element composition (Th = 67.38 ± 45.37 ppm, Nb = 143.19 ± 96.77 ppm, Zr = 814.35 ± 554.98 ppm, Fig. 4g and h). The ratios of the other HFSE to Th are constant (Zr/Th = 12.07 ± 0.41, Nb/Th = 2.12 ± 0.12 and the LREE are enriched compared to the HREE, with La/Yb = 25.29 ± 3.11.

4.1.3.2. Reworked layers in DED 87-08. Tephra layers DED-C, G, H and I are all characterised by sandy and heterogeneous clasts, comprising volcanic materials but also abundant fragments of shells of various marine organisms, as illustrated in Fig. S1 (a, b, c and d; Supplementary Material). Specifically, they include both angular and rounded volcanic particles (e.g., pumices and crystals), planktonic foraminifera, ostracods, gastropods, sea urchin spines and numerous broken pieces of bivalve shells (Figs. S1a–S1d; Supplementary Material). The presence of a biogenic component including organisms that derive from a shallow-water environment suggests that secondary processes may have played a role in their deposition. This interpretation is further supported by their heterogeneity in terms of geochemical glass composition, including both a CF and an Ischia component, as detailed in the following

(Figs. S1e and S1f; Supplementary Material). Overall, these lithological features strongly suggest a reworked origin for these tephra layers.

DED-C (10.78–10.83 m) is ~5 cm-thick and appears light brown to ochre in colour. The few well-preserved glass shards found in this level show a quite heterogeneous composition, with SiO_2 content ranging between 58.70 wt% and 62.30 wt% and a quite homogenous alkali sum, but with variable K_2O and Na_2O contents and ratios (Fig. S1f; Supplementary Material). DED-C is very heterogeneous in terms of incompatible trace element composition (Th = 69.10 ± 43.66 ppm, Nb = 138.78 ± 75.27 ppm, Zr = 866.78 ± 583.73 ppm, Figs. S1g and S1h; Supplementary Material). The ratios of the other HFSE to Th are constant (Zr/Th = 12.50 ± 1.63, Nb/Th = 2.01 ± 0.28) and the LREE are enriched compared to the HREE, with La/Yb = 23.25 ± 5.02.

DED-G (10.98–11.00 m) layer, light brown in colour, shows a heterogeneous composition, with a SiO_2 content between 57.86 and 64.91 wt% and alkali sum between 11.50 and 14.46 wt% that spans the field between phonolites and trachytes. Specifically, three distinct populations can be found: (i) a very low alkali ratio (<1) trachyte, with a low CaO content (~1 wt%), (ii) a trachyte-phonolite with a low alkali ratio (~1.2–1.3) and a CaO content of ~1.8 wt% and (iii) a high alkali ratio (>2) trachyte-phonolite with a CaO content ranging between ~2.0 and 3.0 wt% (see Supplementary Material S1 and Fig. S1). DED-G displays a large heterogeneity also in terms of incompatible trace element composition (Th = 44.01 ± 49.40 ppm, Nb = 90.62 ± 95.20 ppm, Zr = 527.78 ± 626.65 ppm, Figs. S1g and S1h; Supplementary Material). The ratios of the other HFSE to Th is fairly constant (Zr/Th = 11.99 ± 1.59, Nb/Th = 2.06 ± 0.19) and the LREE are enriched compared to the HREE, with La/Yb = 25.23 ± 5.12.

Layers **DED-H and DED-I** (11.14–11.17 m), likely forming an individual layer, are similar in their light brown colour, their textural features and geochemical composition. Like layer DED-G, both DED-H and DED-I are characterised by three distinct populations: (i) a very low alkali ratio (<1) trachyte, with a low CaO content (~1 wt%), (ii) a trachyte-phonolite with a low alkali ratio (~1.2–1.3) with a CaO content of ~1.5–1.8 wt% and (iii) trachyte-phonolite with a high alkali ratio, ranging from 1.84 to 2.55, with a CaO content ranging between 2.14 wt % and 2.91 wt% (see Supplementary Material S1 and Fig. S1). DED-H and DED-I are largely heterogeneous in terms of incompatible trace element composition (Th = 34.13 ± 35.28 ppm, Nb = 69.14 ± 71.53 ppm, Zr = 423.28 ± 480.72 ppm and Th = 47.99 ± 47.59 ppm, Nb = 99.02 ± 81.68 ppm, Zr = 612.97 ± 623.74 ppm, respectively, Figs. S1g and S1h; Supplementary Material). The ratios of the other HFSE to Th are fairly constant (Zr/Th = 12.24 ± 2.19, Nb/Th = 2.03 ± 0.80 and Zr/Th = 12.73 ± 1.41, Nb/Th = 2.06 ± 0.44, respectively) and the LREE are enriched compared to the HREE, with La/Yb = 24.20 ± 7.35 and La/Yb = 24.18 ± 6.51, respectively.

4.1.4. Suhia Kladenetz (SK) quarry (Bulgaria)

The sample **SK-III** (20 cm thick) is light brown in colour. It is compositionally heterogeneous, ranging from the phono-tephritic to tephri-phonolitic compositional fields of the TAS diagram, displaying a mean SiO_2 content of 53.96 ± 3.74 wt% and alkali sums of 10.58 ± 1.88 wt% (Fig. 4a and b). CaO/FeO values are variable, spanning the range between 0.94 and 1.15 and Cl content is variable from 0.28 to 0.51 wt%, with a mean K_2O/Na_2O ratio of 1.69 ± 0.15.

4.2. Grain-size analyses

Grain-size analyses were performed on a variety of samples from terrestrial and marine settings (Table S2, Supplementary Material), thus adding new grain-size analyses to the data already presented by Di Vito et al. (2008) for proximal-medial samples. These analyses highlight the variability of the samples in terms of the coarse/fine fraction ratio and of statistical parameters from medium to distal locations. Fig. 1 displays the dispersal area of all the eruptions, showing how thickness and mean values vary with distance from the volcanic source (Fig. S2; Supplementary Material). The grain-size distribution was analysed for volcanological purposes, and the samples chosen for the investigation are reported in Table S2 (Supplementary Material). In this study we provided the relationship between the distance from the source, the mean values (reported as logarithmic values calculated using the Folk and Ward method; Folk and Ward, 1957) and the tephra layers thickness (Fig. S2; Supplementary Material). Fig. S2 compares the new grain-size data acquired in this study and the grain-size data from Di Vito et al. (2008) as well. The full dataset can be found in the Supplementary Material S2.

Overall, the samples show an inverse trend of the average grain-size M_z *vs* thickness, that varies slightly or abruptly with distance according to the maximum distance reached by the different eruptions. The thickness decreases with increasing distance from the source as expected in distal locations, and M_z increases to high φ values in a direct proportion to the number of fine particles found in distal settings.

4.3. $^{40}Ar/^{39}Ar$ dating

$^{40}Ar/^{39}Ar$ dating results are presented as probability diagrams in Fig. 5. Weighted mean age uncertainties are reported at 2σ, including J uncertainty, and were calculated using Isoplot 4.0 (Ludwig, 2003). All the analytical data can be found in Supplementary Material S3.

4.3.1. S16 29.5–30.0 m

19 single sanidine crystals were dated from the S16 29.5–30.0 sample. 15 out of the 19 crystals display the same age, within uncertainties. The other four crystals are much older, ranging from about 111 ka up to 373 ka. Based on the 15 individual ages of the main population a precise weighted mean age of 106.2 ± 0.4 ka (MSWD = 0.7, p = 0.9; Fig. 5a) was calculated. The corresponding inverse isochron has a spreading of 71.2 % and an atmospheric intercept (i.e., 301 ± 3.8).

4.3.1.1. CET1 10-14. Since sanidine crystals extracted from the CET1 10–14 sample were too small (<300 μm) to perform single-crystal laser fusion, we analysed two crystals at a time. We made a total of 19 measurements for this sample. The probability diagram (Fig. 5b) obtained is simple (i.e., Gaussian) suggesting that all the crystals we dated present a similar age, within uncertainty. We calculated a weighted mean age of 90.4 ± 1.6 ka (MSWD = 0.4, p = 1.0). The corresponding inverse isochron displays a 75% spreading and an atmospheric intercept (i.e., 299.4 ± 1.2).

4.3.1.2. CSP2-A, B, C. 19 single crystals for each sample collected from unit CSP2 (-A, -B and –C) were individually dated (see full dataset in Supplementary Material S3). Excluding 6 crystals that display older ages and that we interpret as xenocrysts, all crystals from the samples shared the same age, as shown by the probability diagram (Fig. 5c). We calculated a weighted mean age of 93.0 ± 0.4 ka (MSWD = 0.7, p = 0.9) using 45 out of the 48 crystals, after excluding the ones with less than 5% radiogenic Ar*. An inverse isochron was built using the 45 single crystals, which demonstrates a 100% spreading, allowing to calculate a very precise initial $^{40}Ar/^{36}Ar$ intercept of 298.7 ± 0.8, which is indistinguishable from the current atmospheric composition.

4.3.1.3. Reworked level DED-C (DED87-08 core). Excluding the plagioclase crystals that gave abnormal older age (see Supplementary Material S3) single sanidine crystals ages ranged from 100 to 117 ka. The probability diagram is complex, showing two main age populations (Fig. 5e). The main population of crystals (11/17) allowed us to calculate a weighted mean age of 101.6 ± 1.4 ka (MSWD = 0.2, p = 1.0). Due to the complexity of the probability diagram, we cannot conclude that this age is the deposition age of level C. Moreover, we could notice that the inverse isochrone corresponding to this younger population of crystals has a 63% spread, with a $^{40}Ar/^{36}Ar$ initial intercepts within uncertainty

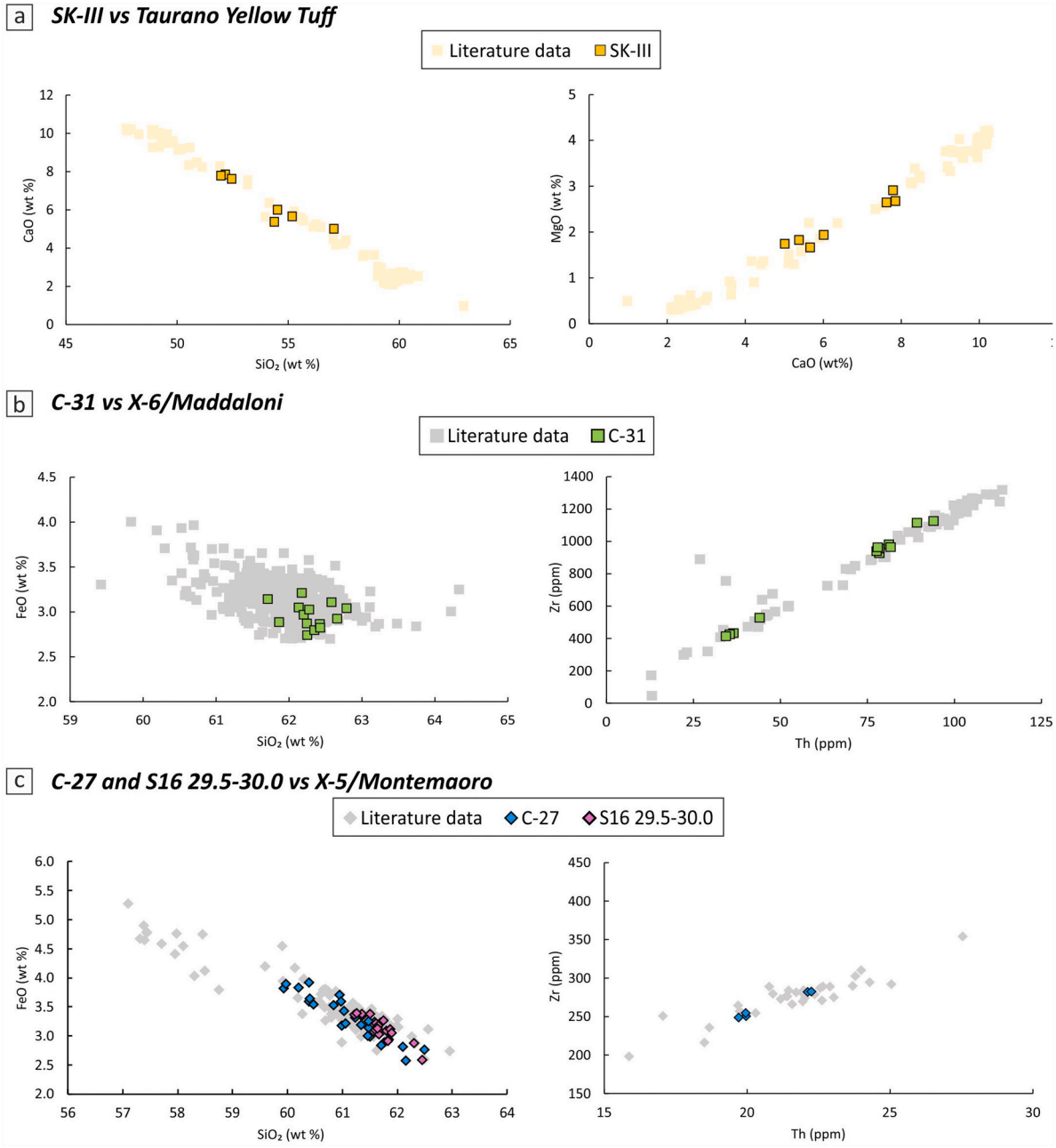

Fig. 6. Comparison between the investigated SK-III, C-31, C-27 and S16 29.50-30-00 and their equivalents. **a)** Major element composition of SK-III in comparison with literature data available for the Taurano Yellow Tuff, including sample AF-YI-13 (Amato et al., 2018) from the Taurano Ignimbrite of Rolandi et al. (2003); Fucino TF-17 (Giaccio et al., 2017b); Campo Felice CF-V5 (Giraudi and Giaccio, 2017); Lake Ohrid OH-DP-0624/OH-DP-0435 (Leicher et al., 2016); OT0701-7 (Sulpizio et al., 2010); Adriatic Sea PRAD3225 (Bourne et al., 2015). **b)** Major and trace element composition of C-31 in comparison with literature data available for X-6/Maddaloni, including Campanian Plain-Maddaloni (Monaco et al., 2022a); Lake Ohrid OH-DP-0435 (Leicher et al., 2021), OT0702-9 (Sulpizio et al., 2010), JO-575 (Caron et al., 2010); Cilento CIL2 (Giaccio et al., 2012), SM1, SM2, SA (Marciano et al., 2008), LeS2 (Donato et al., 2016); Calabria Ta (Donato et al., 2016); Salina Island SAL I (Lucchi et al., 2013); Sulmona POP4 (Regattieri et al., 2015); Lago Grande di Monticchio TM-27 (Wulf et al., 2012); Cavallo Cave G (Zanchetta et al., 2018); Adriatic Sea PRAD2812 (Bourne et al., 2015); Ionian Sea I-9 (Insinga et al., 2014), and 964A-2H-1-45.5 (Vakhrameeva et al., 2021); Tyrrhenian Sea T1 (Iorio et al., 2014); San Gregorio Magno S10 (Munno and Petrosino, 2007); Tenaghi Philippon TP05-27.915 (Wulf et al., 2018); Fucino TF-13 (Giaccio et al., 2017b); Aegean Sea LC21-7.915 (Satow et al., 2015). **c)** Major and trace element composition of C-27 and S16 29.5-30.0 in comparison with literature data available for X-5/Montemaoro, including Campanian Plain SC2-b (Di Vito et al., 2008) Sulmona POP3 and Cilento CIL1 (Giaccio et al., 2012); Tyrrhenian Sea CET1-18 (Petrosino et al., 2016); Cilento LeS1 (Donato et al., 2016); San Gregorio Magno S11 (Munno and Petrosino, 2007); Fucino TF-12 (Giaccio et al., 2017b); Lago Grande di Monticchio TM-25 (Wulf et al., 2012).

equivalent to the atmosphere suggesting that the dated crystals do not contain trapped excess argon.

5. Discussion

5.1. Tephra sources and correlations

In terms of classification, according to the *Total Alkali vs Silica* (Le

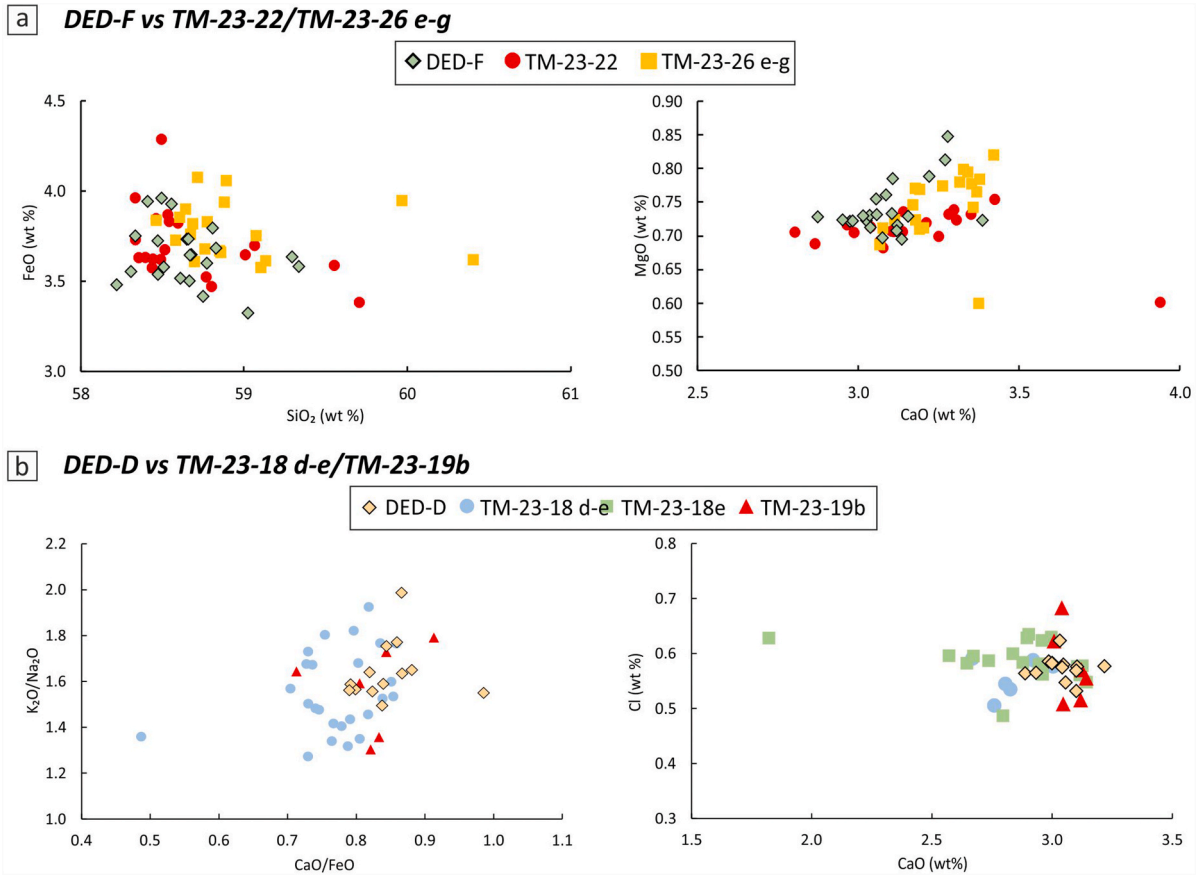

Fig. 7. Comparison between the investigated DED-F and DED-D and their equivalents. **a)** Major element composition of DED-F in comparison with the Monticchio tephras TM-23-22/TM-23-26e-g (Wulf et al., 2004). **b)** Major element composition of DED-D in comparison with the Monticchio TM-23-18d-e/TM-23-19b (Wulf et al., 2004).

Maitre et al., 2002) diagram, almost all the samples investigated in this study cluster on the boundary between the phonolite and trachyte fields, except for samples SK-III and P-10, that display phono-tephritic/tephri-phonolitic and rhyolitic compositions, respectively (Fig. 4a and b). With the exception of P-10, their overall major element composition matches that of the Neapolitan volcanoes (Fig. 4), specifically the relatively high content of Cl (generally >0.3 wt%) and the low CaO/FeO values (i.e., <1), are consistent with the Campi Flegrei and Ischia volcanic sources (Giaccio et al., 2017b) (e.g., Fig. 4c).

Typically, the most evolved Campi Flegrei pyroclastic products are trachytes-phonolites, which can exhibit either a high or low alkali ratio (i.e., K_2O/Na_2O), ranging from ~3 (HAR) to ~1 (LAR). In some cases, LAR and HAR trachytes-phonolites can co-exist in the products of individual CF eruptions, as for the notable case of the CI eruption (e.g., Smith et al., 2016). In contrast, the glasses from Ischia's most evolved products are largely LAR trachytes-phonolites. Despite a similar alkali ratio and classification in the TAS diagram, the Ischia LAR trachytes-phonolites can be reliably discriminated from the CF products using specific oxide concentrations and ratios (e.g., CaO, TiO_2, CaO/FeO, TiO_2/MgO) (Tomlinson et al., 2012, 2014; Giaccio et al., 2017b; Monaco et al., 2022a). Here, we used the CaO/FeO vs Cl diagram (i.e., Giaccio et al., 2017b), which quite successfully distinguishes the glass compositions of Ischia and Campi Flegrei glass compositions (Fig. 4c). In particular, CaO/FeO ratio in CF LAR trachytes-phonolites is higher than those of Ischia at the same Cl content (Fig. 4c). Moreover, trace element composition can support the source correlations, considering that the CF products show slightly lower Zr values than Ischia glass compositions at overlapping Th content (Fig. 4g and h). Using these distinguishing compositional features, samples C-22, C-27, C-31, DED-B, D, F, L, M, N, CSP2, 3 and SK-III can all be attributed to the Campi Flegrei, while DED-E and C-26 are attributed to Ischia.

Finally, P-10 represents a case aside, since its peculiar rhyolitic composition (i.e., comendite-like) allows us to unambiguously attribute it to the activity on Pantelleria island (Fig. 4).

5.1.1. *Campi Flegrei tephra*

SK-III – Taurano Yellow Tuff 159.4 ± 1.6 ka. The position of the SK-III layer in MIS 6 loess L2 gave an estimated age of ~163.9 ka based on the correlation between the magnetic susceptibility and LR04 record (Jordanova et al., 2022). Moreover, the same tephra layer (present as cryptotephra) was recognized in the magnetic susceptibility records from the Kaolinovo site (Northeastern Bulgaria; Balescu et al., 2020) where a sample from L2 loess below the cryptotephra was dated to 167 ± 7 ka and in the Harletz sequence (Northwestern Bulgaria; Lomax et al., 2019) where a sample from L2 loess above the cryptotephra has an estimated age of 171 ± 14 ka. The composition of the MIS 6 SK-III is quite heterogeneous and matches that of Neapolitan volcanoes, with an affinity for Campi Flegrei volcanic products (Fig. 4). SK-III matches part of the wide compositional range characterising the Taurano Yellow Tuff (TYT, De Vivo et al., 2001), whose products were found in several proximal and mid-distal settings (Fig. 1), dated to 160.2 ± 2.0 ka (recalculated; De Vivo et al., 2001). The TYT was correlated to the Fucino tephra TF-17, dated to 159.4 ± 1.6 ka (Giaccio et al., 2019 and references therein), and other equivalent tephras in the Campanian area (S11-PAUP, Amato et al., 2018), in the Campo Felice basin (central Italy, CF-V5; Giraudi and Giaccio, 2017), the Adriatic Sea (PRAD3225; Bourne et al., 2015) and Lake Ohrid (OH-DP-0624 and OT0701-7; Sulpizio et al., 2010; Leicher et al., 2016, 2019). Considering the general consistency of

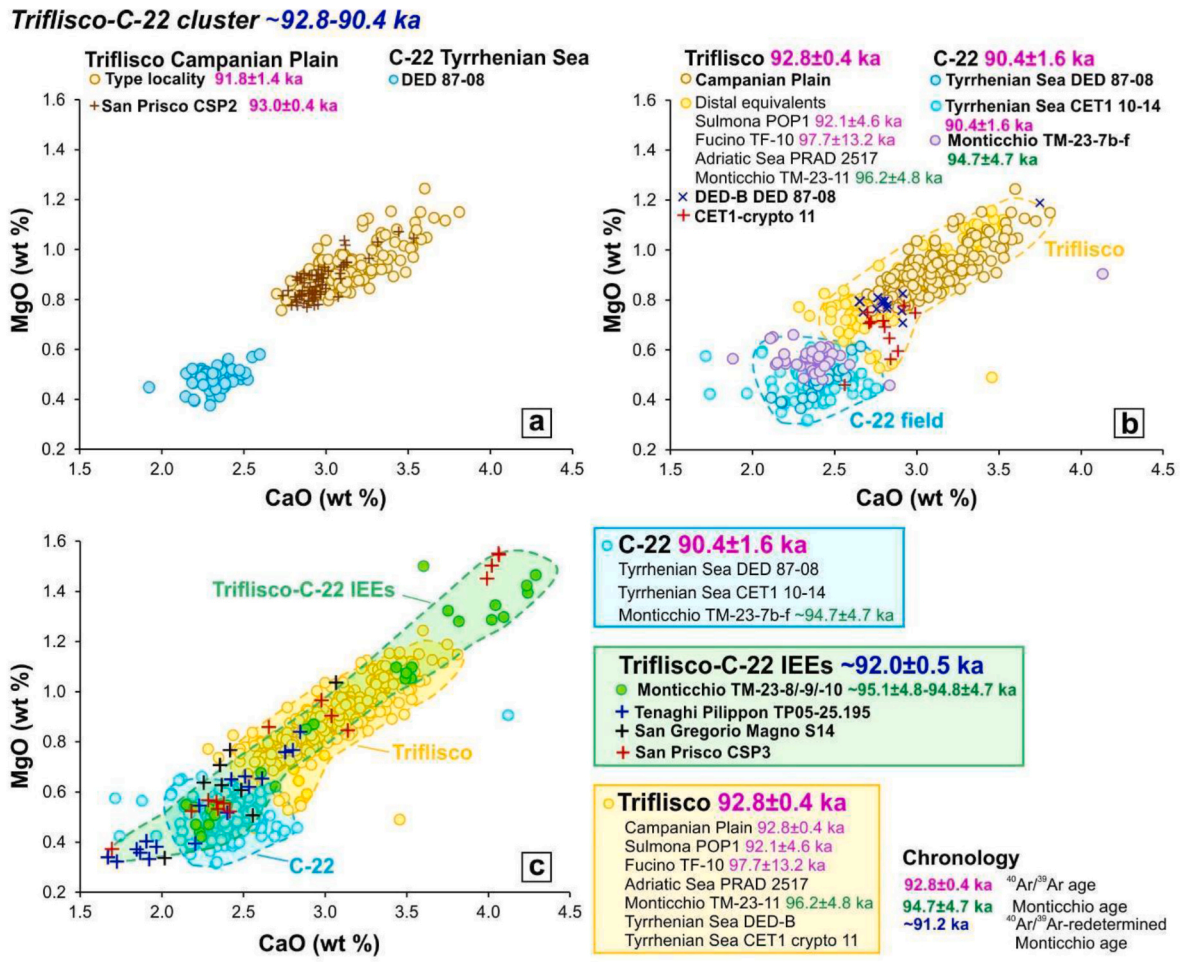

Fig. 8. Compositional features in the CaO vs MgO discriminating diagram, age and apportionment of the Triflisco-C-22 tephra cluster. **a)** Comparison of Triflisco unit with San Prisco CSP2 unit and with C-22 from DED 87-08. **b)** Comparison between Triflisco, including San Prisco CSP2, and C-22 distal counterparts, from Sulmona, Fucino, Adriatic Sea core PRAD1-2, Monticchio and Tyrrhenian Sea core DED 87-08 records, Tyrrhenian Sea core CET1 and Monticchio records, respectively. **c)** Comparison of Triflisco-C-22 Inter-Eruptive Events (IEEs) from Monticchio (i.e., TM-23-8/-9/-10) with San Prisco CSP3, Tenaghi Philippon TP-08-25.195, and San Gregorio Magno S14. The compositional fields of Triflisco (and equivalents) and C-22 (and equivalents) are shown as well. Data sources: C-22, DED-B, CSP2 and CSP3 (glass-WDS): this study; Triflisco type locality (glass-WDS): Monaco et al. (2022a); CET1 10–14 and CET1 crypto-11 (glass-EDS): Petrosino et al. (2016); Monticchio TM-23-11, TM-23-8-/9/-10 and TM-23-7a-f (glass-WDS): Wulf et al. (2004, 2012); Adriatic Sea PRAD 2517 (glass-WDS): Bourne et al. (2015); Tenaghi Philippon TP-05 25.195 (glass-WDS): Wulf et al. (2018).

the stratigraphic position, the age and the geochemical composition of SK-III, which perfectly aligns along the TYT variation trend (Fig. 6a), the TYT represents the most probable candidate for the correlation with SK-III.

Pending additional supporting data, the potential correlation provided in this study highlights the dispersal of the TYT to ultra-distal areas (i.e., Central North Bulgaria, ~900 km from the CF area) and may have important implications for future numerical modelling and magnitude quantification.

C-31 – Maddaloni/X-6 109.3 ± 1.0 ka. Tephra layer C-31 from the Tyrrhenian Sea has been previously associated to Campi Flegrei and correlated to tephra layers outcropping in mid-proximal and distal settings, including Lake Ohrid (OH-DP-0435, Leicher et al., 2021; OT0702-9, Sulpizio et al., 2010; JO-575, Caron et al., 2010), Cilento (CIL2, Giaccio et al., 2012; SM1, SM2, SA, Marciano et al., 2008; LeS2, Donato et al., 2016), Calabria (Ta, Donato et al., 2016), Salina Island (SAL I, Lucchi et al., 2013), Sulmona basin (POP4, Regattieri et al., 2015), Lago Grande di Monticchio (TM-27, Wulf et al., 2012), Cavallo Cave (G, Zanchetta et al., 2018) Adriatic Sea (PRAD2812, Bourne et al., 2015), Ionian Sea (I-9, Insinga et al., 2014; 964A-2H-1-45.5, Vakhrameeva et al., 2021), Tyrrhenian Sea (T1, Iorio et al., 2014), San Gregorio Magno (S10, Munno and Petrosino, 2007), Tenaghi Philippon (TP05–27.915, Wulf et al., 2018), Fucino basin (TF-13, Giaccio et al., 2017b), and Aegean Sea (LC21–7.915, Satow et al., 2015). Recently, Monaco et al. (2022a) found another correlative in the Campanian Plain (i.e., Maddaloni unit), whose composition matches that of the X-6 eruption (109.3 ± 1.0 $^{40}Ar/^{39}Ar$ ka, Monaco et al., 2022a; 109.4 ± 5.5 varve age; Wulf et al., 2012). Sample C-31 (bottom and top) was analysed here for the first time using EMPA-WDS. The glass from the sample at the bottom is predominantly a CF LAR trachyte with a minor CF HAR trachyte component (see Supplementary Material S1). The second composition occurring in the uppermost sample of C-31 layer is instead a typical Ischia trachyte, as clearly inferable from the very low CaO content (see Supplementary Material S1). The CF component of the C-31, including the coexistence of both LAR and HAR trachytes, is fully consistent with the composition of the X-6 marine tephra and its counterparts in both mid-proximal and distal terrestrial records (Fig. 6b) and confirms the previously proposed correlation with X-6/Maddaloni eruption (for more detailed information on the data source, the reader is referred to Table S1, Supplementary Material). The Ischia LAR trachyte component, found only on the top of the C-31 layer, can be instead considered contamination related to bioturbation processes of volcanic material from an Ischia eruption.

C-27 and S16 29.5-30.0 m – Montemaoro/X-5 106.24 ± 0.35 ka.

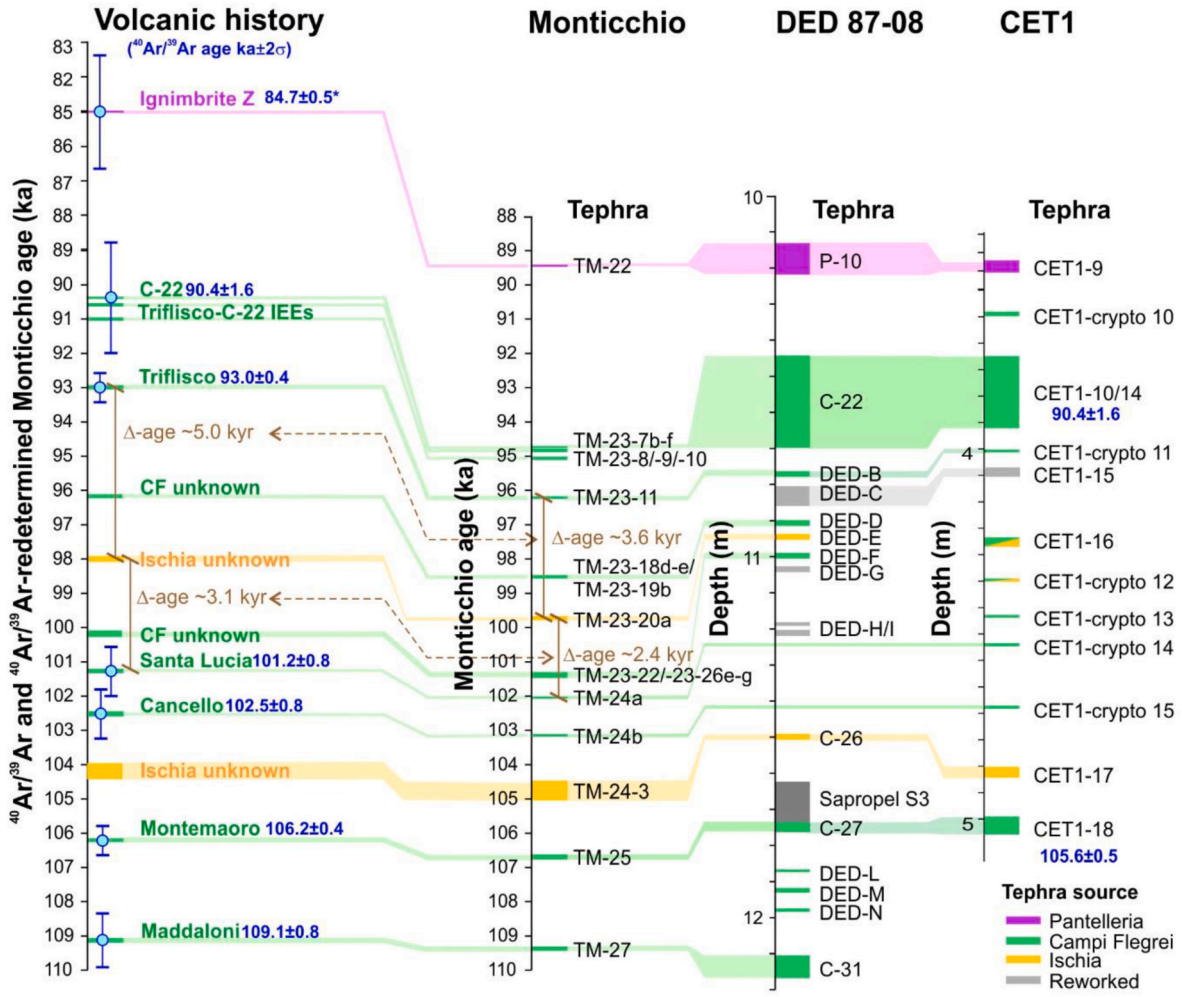

Fig. 9. Correlation between Monticchio tephra time-series with Tyrrhenian DED 87-08 and CET1 depth-series. The left timescale ($^{40}Ar/^{39}Ar$ and $^{40}Ar/^{39}Ar$-redetermined Monticchio age) is based on the available $^{40}Ar/^{39}Ar$ geochronology of the tephra markers and, when not available, on the combination of the $^{40}Ar/^{39}Ar$ geochronology and Δ-Monticchio age. *The age of Ignimbrite Z is referred to an unpublished paper cited in Rotolo et al. (2013) and was not considered for the age model provided in this study. Specifically, the age of a $^{40}Ar/^{39}Ar$-undated tephra is determined by linearly redistributing, within the $^{40}Ar/^{39}Ar$-based time-scale, the age differences, according to the Monticchio chronology, between the $^{40}Ar/^{39}Ar$-undated tephra and the two $^{40}Ar/^{39}Ar$ dated tephra lying immediately below and above the undated one (Δ−age, see the examples for TM-237b-f and TM-23-20a shown in figure).

The marine layer C-27 was previously ascribed to the marker tephra X-5 (Paterne et al., 2008; Giaccio et al., 2012; Petrosino et al., 2016) and correlated to tephra layers from the Campanian Plain (SC2-b, Di Vito et al., 2008) Sulmona Basin (POP3, Giaccio et al., 2012), Cilento (CIL1, Giaccio et al., 2012; LeS1, Donato et al., 2016), Tyrrhenian Sea (CET1-18, Petrosino et al., 2016), San Gregorio Magno (S11, Munno and Petrosino, 2007), Fucino basin (TF-12, Giaccio et al., 2017b), and Lago Grande di Monticchio (TM-25, Wulf et al., 2012). It was dated to 105.6 ± 0.5 ka using $^{40}Ar/^{39}Ar$ dating (Petrosino et al., 2016) and the associated varve age is 106.7 ± 5.3 ka (Wulf et al., 2012). Based on published EDS data, Monaco et al. (2022a) found a correlative in the Campanian Plain (i.e., Montemaoro unit), whose composition matches that of the X-5 eruption. The WDS-glass composition provided for C-27 confirms the previous attributions. Specifically, the glass from C-27 is a typical CF HAR trachyte, matching, in terms of trace elements as well, the composition of X-5 and its equivalents in both mid-proximal and distal terrestrial records (Fig. 6c).

The glass from layer S16 29.5–30.0 also matches that of the X-5/Montemaoro published composition (Fig. 6c). The geochemical correlation is strongly supported by the new $^{40}Ar/^{39}Ar$ data obtained for S16 29.50–30.0 (106.24 ± 0.35 ka, Fig. 5a), which is indistinguishable from those of the Tyrrhenian Sea CET1-18 (105.6 ± 0.5 ka, Petrosino et al., 2016) and Sulmona POP3 (106.2 ± 1.3 ka; Giaccio et al., 2012) tephra, correlated to the Maddaloni/X-5 unit. Noteworthy, the glass-WDS geochemical composition and the $^{40}Ar/^{39}Ar$ dating we obtained in this study for the S16 29.5–30.0 tephra in the Campanian plain provide the most proximal dataset for the CF Montemaoro unit.

DED-L, M and N – Campi Flegrei unknown >106 ka – <109 ka. These three CF layers stratigraphically occur between Maddaloni/X-6 (109.3 ± 1.0 ka; Monaco et al., 2022a) and Montemaoro/X-5 (106.24 ± 0.35 ka, Fig. 5a). DED-L and DED-N are LAR trachites-phonolites, while DED-M is a CF HAR trachyte-phonolte. Currently, none of these layers can be ascribed to specific eruptions as they have not been previously recognized in the CF or in distal settings such as Lago Grande di Monticchio (e.g., Wulf et al., 2004), Sulmona Basin (e.g., Regattieri et al., 2015, 2017) or in the Adriatic Sea (e.g., Bourne et al., 2015). However, the presence of these tephra records indicates a more complex history between the major eruptions of Maddaloni/X-6 and Montemaoro/X-5.

DED-F – TM-23-22/TM-23-26 e-g – Campi Flegrei unknown. The DED-F tephra is a CF LAR phonolite, with a relatively high content of CaO (~3.1 wt% in average) with respect to the Ischia glass. A tentative correlation with the distal Monticchio record is proposed here (Fig. 7a). Specifically, we explored potential correlatives taking into consideration

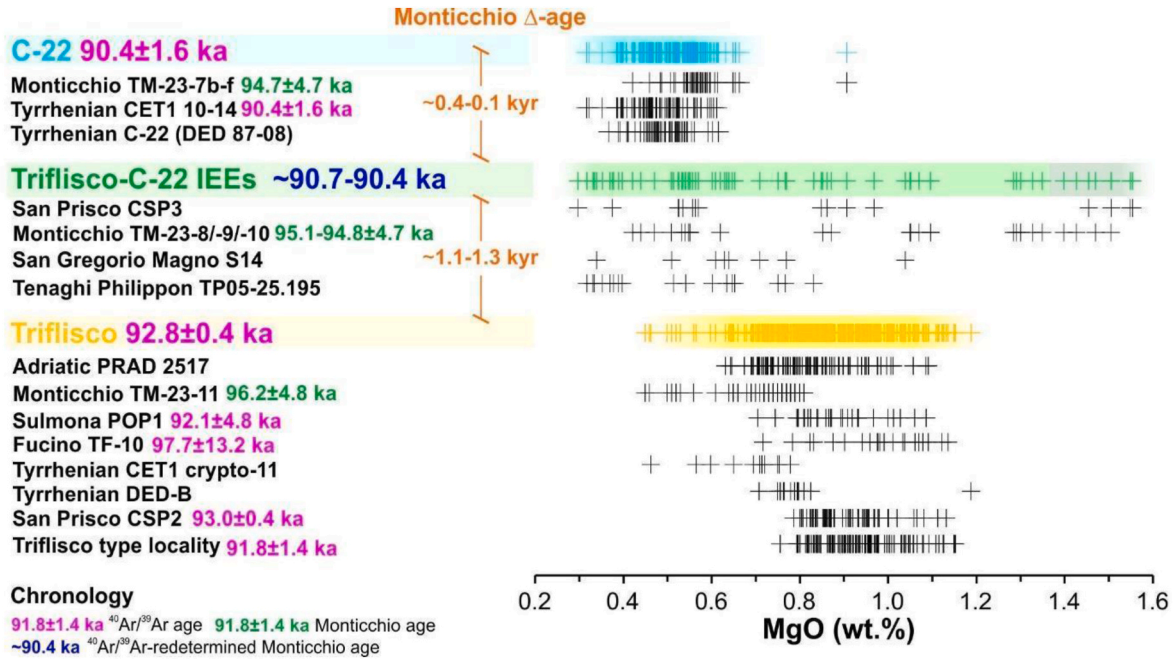

Fig. 10. Variability and degree of evolution of the products of the Triflisco-C-22 tephra cluster as revealed by the content of MgO in tephra glass. Data sources: C-22, DED-B, CSP2 and CSP3 (glass-WDS): this study; Triflisco type locality (glass-WDS): Monaco et al. (2022a); CET1 10–14 and CET1 crypto-11 (glass-EDS): Petrosino et al. (2016); Monticchio TM-23-11, TM-23-8-9-10 and TM-23-7a-f (glass-WDS): Wulf et al. (2004, 2012); Adriatic Sea PRAD 2517 (glass-WDS): Bourne et al. (2015); Tenaghi Philippon TP-05 25.195 (glass-WDS): Wulf et al. (2018).

the stratigraphic position of the DED-F, which lies between C-22 and C-27. In this stratigraphic interval of Monticchio record, tephra layers TM-23-22 and TM-23-26 e-g, dated to 100.2 ± 5.0 ka and 101.6 ± 5.1 ka, respectively (Wulf et al., 2012), match quite well the major element composition of DED-F (Fig. 7a). However, based on the available data, a definitive correlation for the DED-F with one of these layers is currently untenable.

DED-D – TM-23-18 d-e/TM-23-19b – Campi Flegrei unknown. Tephra sample DED-D is a moderately HAR (1.65 on average) CF trachyte. A tentative correlation with the Monticchio record is proposed here as well, by exploring the same stratigraphic interval between C-22 and C-27 equivalents. We attempted some correlations using major element composition, and we found two potential correlation candidates that show a good overlap with the DED-D composition, i.e., TM-23-18d-e and TM-23-19b, dated to 98.5 ± 4.9 and 98.6 ± 4.9 ka, respectively (Wulf et al., 2012) (Fig. 7b). Yet, as for the DED-F layer, a correlation of the DED-D tephra layer to a specific Monticchio tephra is not possible at this stage. However, considering the strict stratigraphic and chronological proximity of TM-23-18d-e and TM-23-19b (~98.5 ka and 98.6 ± 4.9 ka, respectively), DED-F is likely derived from the deposition of both Monticchio tephra.

The Triflisco-C-22 eruption cluster ~92.8 ± 0.4-90.4 ± 1.6 ka. Based on the lithological features, the San Prisco unit CSP2 has been identified in this study as a new occurrence in the Campanian Plain of the Triflisco unit (Monaco et al., 2022a). This attribution is fully supported by the chemical composition and the new $^{40}Ar/^{39}Ar$ dating at 92.96 ± 0.41 ka (Fig. 5c), which is indistinguishable from that previously obtained for the Triflisco Plinian fall collected at the type locality (91.8 ± 1.4 ka; Monaco et al., 2022a) but with a higher precision. The combination of the high-precision dating of CSP2 with the previous age determination obtained for Triflisco yields a final age of 92.78 ± 0.38 ka (Fig. 5d). According to Monaco et al. (2022a) the Triflisco Plinian fall represents the most proximal deposit of a CF eruption that generated widespread tephra, representing a relevant stratigraphic and chronological marker in MIS 5 successions of the central Mediterranean and eastern Europe.

Specifically, a correlation of the Triflisco pumice has been proposed for distal tephra (i) PRAD-2517 in Adriatic Sea core PRAD1-2, (ii) CET1 10–14 in the Tyrrhenian Sea core CET1, (iii) TF-10 from the central Italy lacustrine successions of the Fucino, (iv) POP1 from the Sulmona basin, (v) TM-23-11 from Lago Grande di Monticchio, (vi) S14 from San Gregorio Magno, and (vii) cryptotephra TP05–25.195 from the Tenaghi Philippon peat record, in Greece (Fig. 1). Previous investigations (e.g., Giaccio et al., 2012; Petrosino et al., 2016; Wulf et al., 2018) proposed the correlation of some of these distal tephra layers to the Tyrrhenian Sea tephra C-22 as well, hence C-22 was subsequently considered as equivalent to the mid-proximal Triflisco pumice fall (Monaco et al., 2022a). However, the proposed correlation was only based on the mean SEM-EDS glass chemical composition of C-22 available at that time (Paterne et al., 2008), and essentially on general chronological and climatostratigraphic constraints.

Our new glass-WDS data acquired for C-22 in DED 87-08 reveal significant differences with Triflisco tephra, which raises questions about this correlation. Such differences are evident for several major elements (Fig. 8 and Fig. S3, Supplementary Material) but are particularly clear using the CaO vs MgO diagram, which defines two well-distinguished fields defined by Triflisco and C-22 (Fig. 8a). A comparison with many of the Triflisco distal tephra proposed in previous studies reveals that these layers cluster into the two distinct fields of Triflisco and C-22. Specifically, the Sulmona POP1, Fucino TF-10, Adriatic Sea PRAD-2517 and the Monticchio TM-23-11 match the Triflisco composition, while the layer CET1 10–14 from the Tyrrhenian Sea falls in the C-22 field (Fig. 8b).

The notion that Triflisco and C-22 represent two different eruptions is also supported by the new age of the layer CET1 10–14 at 90.4 ± 1.6 ka, equivalent to the C-22, which, despite its relatively large uncertainty, is statistically distinguishable from the age of Triflisco at 92.78 ± 0.38 ka. Furthermore, we observed that the glass from the layer DED-B and CET1 crypto-11, laying immediately below C-22 (Fig. 2d) and its equivalent in core CET1 (CET 10–14; Fig. 9), match the Triflisco composition (Fig. 8b and Fig. S3, Supplementary Material), suggesting a good correlation with the above-mentioned eruption. This highlights

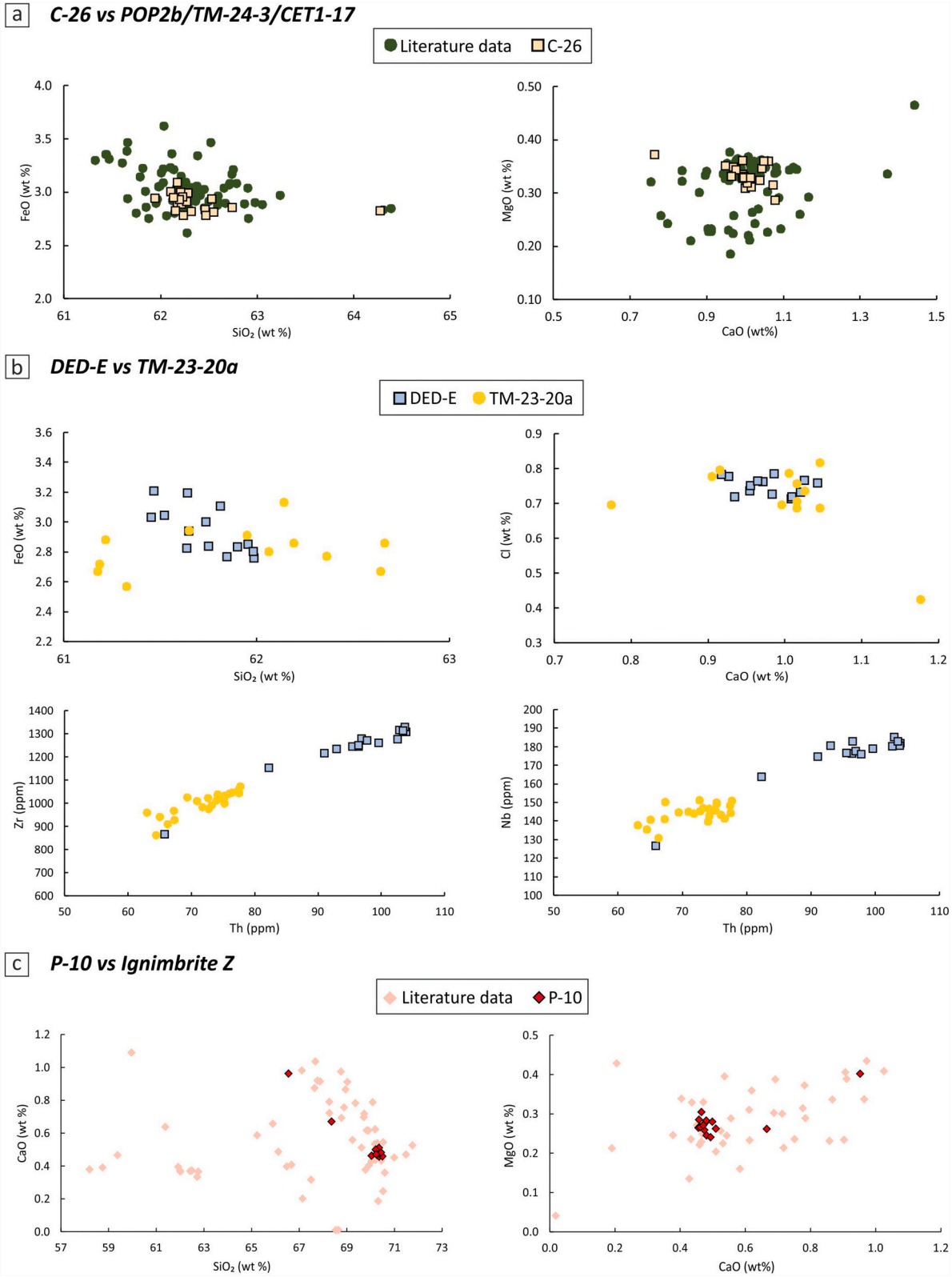

Fig. 11. **a)** Comparison between C-26 and literature data from the POP2b eruption (Giaccio et al., 2012). Data source: C-26 (glass WDS and LA-ICP-MS): this study; literature data for the POP2b eruption: POP2b (Giaccio et al., 2012), CET1-17 (Petrosino et al., 2016) and TM-24-3 (Giaccio et al., 2012; Petrosino et al., 2016). **b)** Comparison between DED-E and TM-23-20a for selected major and trace elements. Data source: DED-E (glass WDS and LA-ICP-MS): this study; Literature data for TM-23-20a (glass WDS and LA-ICP-MS): Tomlinson et al. (2014). **c)** Major element composition of the sample P-10 from DED87-08 (Tyrrhenian Sea) in comparison with literature data of Ignimbrite Z. Data source: P-10 (glass WDS): this study; Literature data: P-10 (Paterne et al., 1988), CET1-9 (Petrosino et al., 2016), PRAD-2375 (Bourne et al., 2015) and TM-22 (Wulf et al., 2004). More detailed data on major/trace element composition can be found in the Supplementary Material S1.

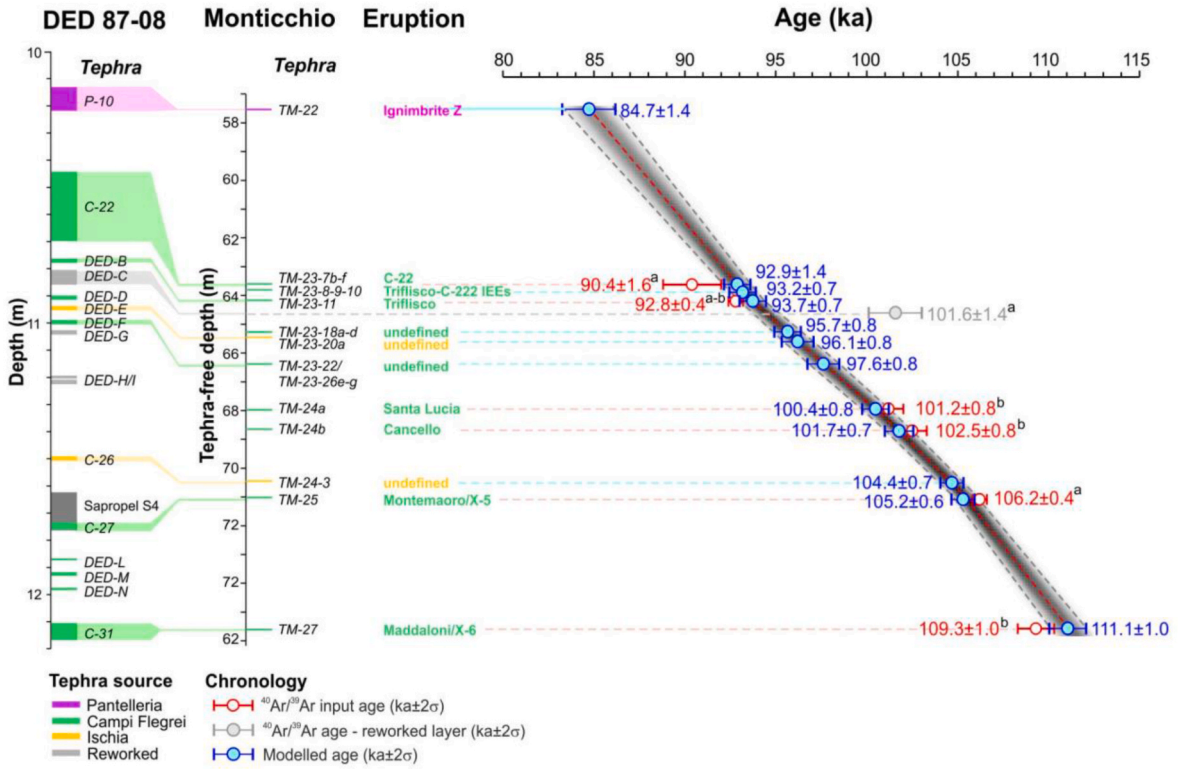

Fig. 12. Bayesian age-depth model for the MIS 5 section of the Lago Grande di Monticchio record and correlation with core DED 87-08 from the Tyrrhenian Sea. $^{40}Ar/^{39}Ar$ dates of correlated tephra layers from the literature and from this study (dates in red) are used as framework for modelling ages of undated tephras (in blue) using incremental varve dates of the Monticchio MON14 chronology by Wulf et al. (2012) and Martin-Puertas et al. (2014). The depths we considered for the age model are tephra-free. $^{40}Ar/^{39}Ar$ data source: [a] This study; [b] Monaco et al. (2022a).

that Triflisco and C-22 are related to two stratigraphically and chronologically different eruptions, with Triflisco being slightly older than C-22 (Fig. 9). We also observed a good chemical match between C-22 and the Monticchio tephra TM-23-7b-f (94.7 ± 4.7 ka, Monticchio age; Wulf et al., 2012), which is stratigraphically and chronologically separated by the Triflisco equivalent TM-23-11 (96.2 ± 4.8 ka, Monticchio age).

Concerning the other two tephra previously associated to Triflisco/C-22, i.e., the Tenaghi Philippon TP05–25.195 and San Gregorio Magno S14 (Monaco et al., 2022a), we note that their compositions cross and extend beyond the envelope of the Triflisco and C-22 fields (Fig. 8c). A similar wide compositional range also features the glass from the San Prisco ash layer CSP3 (Fig. 8c), as well as from the Monticchio tephra layers TM-23-8/-9/-10, which lay in between TM-23-11/Triflisco and TM-23-7b-f/C-22 (Fig. 9). Such a stratigraphic and geochemical consistency (Figs. 8 and 9) would suggest that all these layers could be related to a cluster of eruptions that occurred between the main Triflisco and C-22 events, i.e., the 'Triflisco-C-22 Inter-Eruptive Events', hereafter Triflisco-C-22 IEEs (Figs. 8–10).

Based on this evidence, the Tenaghi Philippon TP05–25.195 and San Gregorio Magno S14 could be either related to the Triflisco-C-22 IEEs (TM-23-8/-9/-10 and CSP3) or be the expression of the deposition of material from multiple eruptions including either all or a part of the Triflisco, Triflisco-C-22 IEEs and C-22 cluster. However, considering the shallow-water setting of the San Gregorio Magno marsh, subject to frequent tephra re-sedimentation processes (Petrosino et al., 2019), and of the Tenaghi Philippon peatland, which are both affected by intense bioturbation (Wulf et al., 2018), the layers from these records, rather than representing the Triflisco-C-22 IEEs, could reflect the whole Triflisco-C-22 eruption cluster.

Summarising, differently from the previous studies, the above evidence supports the notion that the Triflisco-C-22 tephra represents multiple eruptions in the time span of 2.4 ± 1.6 kyr, between 92.8 ± 0.4 $^{40}Ar/^{39}Ar$ ka (96.2 ± 4.8 ka, Monticchio age) and 90.4 ± 1.6 $^{40}Ar/^{39}Ar$ ka (~96.2–97.7 ka, Monticchio age) (Fig. 9).

Though compositionally partially overlapping, the products of these eruptions show distinctive fingerprinting features, especially in terms of the degree and variability of magma evolution, which may allow their discrimination. Overall, Triflisco shows a relatively wide but well-clustered range of compositions, characterised by a MgO content mostly ranging between ~1.0 wt% and ~0.7 wt% (Fig. 10). The Triflisco-C-22 IEEs is instead characterised by the widest and scattered compositional range, with highly variable MgO content ranging between ~1.6 wt% and ~0.3 wt%. Finally, C-22 is characterised by the narrowest compositional variability, with MgO content mostly clustering around 0.5 ± 0.1 wt% (Fig. 10).

5.1.2. Ischia and Pantelleria tephra

C-26 – TM-24-3 - Ischia unknown ~105 ka. C-26 tephra from the Tyrrhenian Sea was studied for the first time by Paterne et al. (2008), it was associated with an Ischia source and correlated to the tephra layers POP2b (Sulmona basin, Giaccio et al., 2012), CET1-17 (Tyrrhenian Sea, Petrosino et al., 2016) and TM-24-3 tephra (Lago Grande di Monticchio, Wulf et al., 2012). Major and trace elements composition obtained in this study confirm this correlation (Fig. 11a). Even though no proximal correlatives on the Ischia Island were found, the above-mentioned tephra layers testify for an eruption event at ~105 ka that is recorded in mid-proximal and distal settings.

DED-E – TM-23-20a – Ischia unknown ~96 ka. Based on its major element chemical composition and its stratigraphic position, between DED-D and DED-F, DED-E can be reliably correlated to the Monticchio Ischia tephra TM-23-20a. The Monticchio equivalent TM-23-20a was dated, according to Monticchio chronology, at 99.7 ± 5.0 ka (Wulf et al., 2012) (Fig. 9). Nevertheless, the trace element composition provided for TM-23-20a by Tomlinson et al. (2014) shows some differences with the

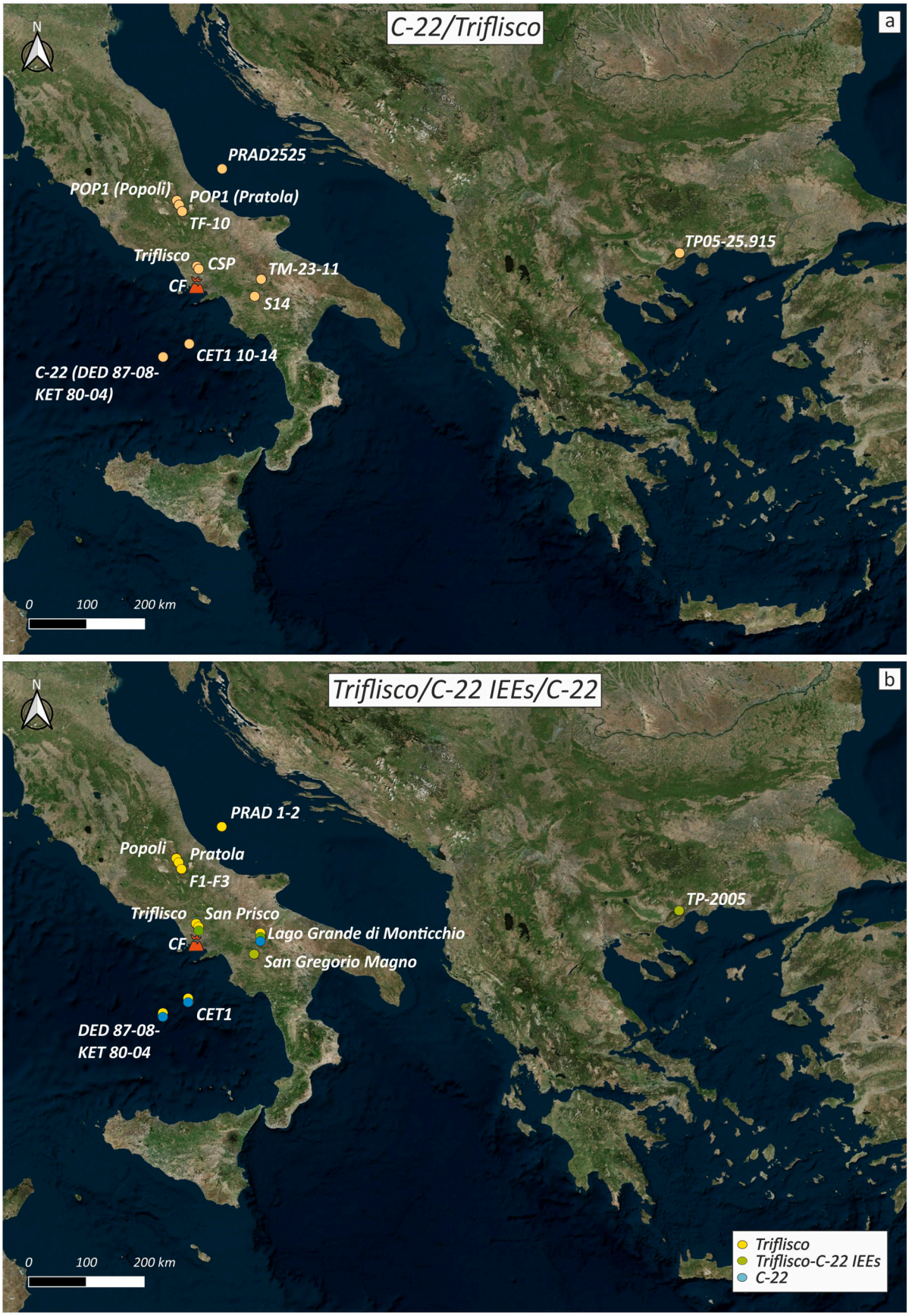

Fig. 13. **a)** Dispersal area of the C-22 eruption according to literature data; **b)** Dispersal area of the Triflisco (yellow dots), Triflisco-C-22 IEEs (green dots) and C-22 (sky-blue dots) according to the new correlations provided in this work.

Table 1
Synthesis of the chronology for the investigated MIS 5 Campi Flegrei and Ischia tephra, including $^{40}Ar/^{39}Ar$ ages, Monticchio varve-supported ages, Monticchio modelled ages and best ages. The $^{40}Ar/^{39}Ar$ ages and the tephra-free depths were used for the Monticchio age-depth model using the Bacon software. Source abbreviations: **P** (Pantelleria); **CF** (Campi Flegrei); **IS** (Ischia).

Source	Terrestrial and marine records		Lago Grande di Monticchio					Best age (ka±2σ)
	Unit/tephra	$^{40}Ar/^{39}Ar$ age (ka ±2σ)	Tephra	Depth base (m)		Monticchio age (ka±2σ)		
				Total	Tephra-free	Varve-supported	Modelled	
P	Ignimbrite Z/P-10		TM-22	59.68	57.61	89.4 ± 4.5[c]	84.7 ± 1.4	84.7 ± 1.4[d]
CF	C-22/CET1 10-14	90.4 ± 1.6[a]	TM-23-7b-f	65.96	63.70	94.7 ± 4.74[c]	92.9 ± 0.8[a]	90.4 ± 1.6[e]
CF	Triflisco-C-22 IEES		TM-23-8/-9/-10	66.24	63.95	95.08 ± 4.7[c]	93.2 ± 0.7[a]	93.2 ± 0.7[d]
CF	Triflisco/DED-B/CET1-crypto11	92.8 ± 0.4[a-b]	TM-23-11	66.60	64.29	96.2 ± 4.8[c]	93.7 ± 0.7[a]	92.8 ± 0.4[e]
CF	DED-D		TM-23-18d-e/TM-23-19b	67.76	65.42	98.5 ± 4.9[c]	95.7 ± 0.8[a]	95.7 ± 0.8[d]
IS	DED-E		TM-23-20a	68.06	65.64	99.7 ± 5.0[c]	96.1 ± 0.8[a]	96.1 ± 0.8[d]
CF	DED-F		TM-23-22/TM-23-26e-g	69.00	66.48	100.2 ± 5.0[c] 101.6 ± 5.1[c]	97.6 ± 0.8[a]	97.6 ± 0.8[d]
CF	Santa Lucia/CET1-crypto14	101.2 ± 0.8[b]	TM-24a	70.73	68.06	102.0 ± 5.1[c]	100.4 ± 0.8[a]	101.2 ± 0.8[e]
CF	Cancello/CET1-crypto15	102.5 ± 0.8[b]	TM-24b	71.75	68.83	103.1 ± 5.2[c]	101.7 ± 0.7[a]	102.5 ± 0.8[e]
IS	C-26/CET1-17		TM-24-3	73.44	70.49	105.0 ± 5.3[c]	104.4 ± 0.7[a]	104.4 ± 0.7*
CF	Montemaoro/X-5/C-27/CET1-18	106.2 ± 0.4[a]	TM-25	74.11	71.04	106.7 ± 5.3[c]	105.2 ± 0.6[a]	106.2 ± 0.4[e]
CF	DED-L							106.2–109.3°
CF	DED-M							106.2–109.3°
CF	DED-N							106.2–109.3°
CF	Maddaloni/X-6/C-31	109.3 ± 1.0[b]	TM-27	78.86	75.76	109.4 ± 5.5[c]	111.1 ± 1.0[a]	109.3 ± 1.0[e]

[a] This study.
[b] Monaco et al. (2022a).
[c] Wulf et al. (2012).
[d] Monticchio modelled age.
[e] 40Ar/^{39}Ar age, ° Estimated age.

DED-E tephra, i.e., an enrichment in Th, Zr and Nb content in DED-E (Fig. 11b). Hence, the correlation between the two layers must remain very tentative.

P-10 – Ignimbrite Z 84.7 ± 0.5 ka. Our new glass-WDS data for tephra layer P-10 reveals the peculiar composition of the Pantelleria products and thus confirms the previous attribution of this layer to Pantelleria Island (Paterne et al., 2008). P-10 was previously correlated with Monticchio tephra TM-22 and associated with the Ignimbrite Z eruption from Pantelleria (Wulf et al., 2004).

P-10 has been further assigned to the Adriatic Sea PRAD-2375 tephra (Bourne et al., 2010) and the CET1-9 layer from the Tyrrhenian Sea core CET1 (Petrosino et al., 2016). Our new glass WDS data of P-10 confirms those correlations, as well as the attribution to Ignimbrite Z (Fig. 11c). The eruption was dated to 79.3 ± 8.4 ka (K/Ar age; Mahood and Hildreth, 1986). Later, paleomagnetic studies on the pre-Green Tuff ignimbrites were carried out by Speranza et al. (2012) and Jordan et al. (2018) and the data were combined with the ages previously proposed by Rotolo et al. (2013), providing an age of 84.7 ± 0.5 ka (Rotolo et al., 2021). However, they refer to an unpublished study (see Rotolo et al., 2013 for details), thus preventing us from considering this age as a reliable one and to use it for the age model.

5.1.3. Reworked layers

The nature of the volcanoclastic layers DED-C, G, H and I from the DED 87-08 core, which has been deduced mainly from their textural features and components (see section 2.2.; Fig. S1, from a to d) is confirmed by the results of the geochemical analyses and $^{40}Ar/^{39}Ar$ dating.

Specifically, the layers DED-G, –H and –I systematically show multiple compositional populations, including CF-like LAR trachites-phonolites, CF-like HAR trachytes-phonolites and Ischia-like LAR trachytes. Indeed, such a geochemical feature, together with the lithological-textural characteristics, strongly suggest that they derive from a mixing due to secondary depositional processes. On the other hand, a mixing by bioturbation of sub-contemporanous eruption from two different sources (i.e., Ischia and CF), as proposed by previous studies (Paterne et al., 2008) and theoretically possible in this context of relatively low sedimentation rate, appears unlikely since such a geochemical mixing is associated with other independent lithological features (i.e., the occurrence of fragments of shallow water shells). In this regard, it is important to note that the DED-E, with a homogenous Ischia signature, and DED-D, with a homogenous CF signature, that are stratigraphically only 3 cm apart from each other, appear lithologically and geochemically distinguished and not affected by any mixing.

Furthermore, the $^{40}Ar/^{39}Ar$ data we obtained for DED-C crystals display two distinct age populations, one centred at around 101.6 ka and another one centred at around 112.0 ka (Fig. 5e), which are both completely inconsistent with the age-depth distribution of the other tephra layers. Indeed, the DED-C layer lies 8 cm below the layer DED-B correlated to Triflisco, dated to ~93 ka, and ~90 cm above C-27, correlated to Montemaoro/X-5, dated to ~106 ka. So, assuming a primary nature of the level DED-C, its age and position would implicate an extreme, unrealistic variability of the sedimentation rates, ranging from ~0.9 cm/ky, between DED-B and DED-C, and ~19.6 cm/kyr, between DED-C and C-27.

Summarising, all these indications consistently suggest that secondary processes may have played a role in the deposition of these layers, likely evolved turbidites, as they may occur in the marine environment (e.g., Freundt et al., 2023). The DED 87-08 marine core is located in a morpho-structure high, probably not subject to landslides coming from the Campanian margin platform (Fig. 3a). However, local mass movements could have occurred, triggered by gravitational instabilities or tectonic processes, rather than the occurrence of contemporaneous eruptions from Campi Flegrei and Ischia, involving products of different ages, as the probability distribution of the dated crystals suggests (Fig. 5e). This new interpretation could be useful to constrain the tempo of secondary processes after explosive eruptions occurred from Campanian volcanoes.

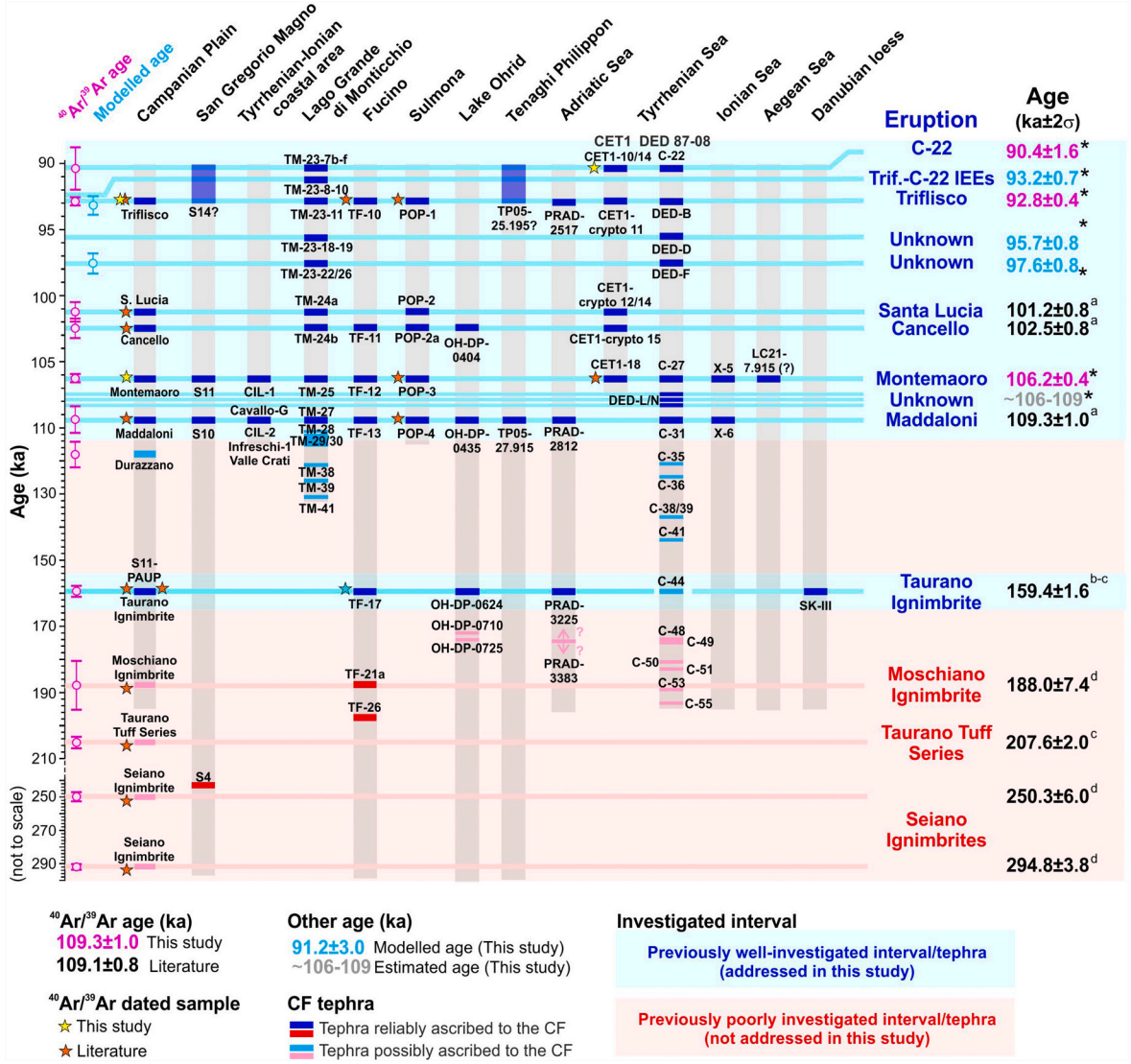

Fig. 14. Synthesis of the Eastern Mediterranean tephrostratigraphy highlighting the occurrence of Campi Flegrei tephra spanning the 290-90 ka interval. Note that the time-scale is not linear. $^{40}Ar/^{39}Ar$ data source: * This study; [a] Monaco et al. (2022a); [b] Giaccio et al. (2017b); [c] De Vivo et al. (2001); [d] Rolandi et al. (2003). Data source for the Campanian Plain: Triflisco, Santa Lucia, Cancello, Montemaoro and Maddaloni: Monaco et al. (2022a); S11-PAUP: Amato et al. (2018); San Prisco and S16: this study; Moschiano Ignimbrite, Taurano Ignimbrite Taurano Tuff Series and and Seiano Ignimbrite: De Vivo et al. (2001) and Rolandi et al. (2003); San Gregorio Magno: Munno and Petrosino (2007), Petrosino et al. (2019); Tyrrhenian-Ionian coastal area: Giaccio et al. (2012), Zanchetta et al. (2018); Lago Grande di Monticchio: Wulf et al. (2012); Fucino basin: Giaccio et al. (2017a) and Monaco et al. (2022b); Sulmona basin: Giaccio et al. (2012), Regattieri et al. (2015); Lake Ohrid: Leicher et al. (2016, 2019, 2021); Tenaghi Philippon: Wulf et al. (2018); Adriatic Sea: Bourne et al. (2015); Tyrrhenian Sea: (DED 87-08): Paterne et al. (2008), this study; (CET1) Petrosino et al. (2016); Ionian Sea: Keller et al. (1978), Vakhrameeva et al. (2021); Aegean Sea: Satow et al. (2015); Danubian loess: Jordanova et al. (2022). For more detailed information the reader is referred to Table S1 (Supplementary Material).

5.1.4. Age model and implications for the chronology of the CF activity at 110-90 ka

The chronological constraints used as input ages for the Bayesian age-depth model are quite well distributed along the MIS 5 interval, and the resulting age-depth curve shows a rather homogenous sedimentation rate in the Monticchio record (Fig. 12). The age of 101.6 ± 1.4 ka of the layer DED-C, which is stratigraphically below the layer DED-B, is instead clearly in conflict with the age-depth model provided in Fig. 12, confirming the interpretation of the reworked origin of layer DED-C and, consequently, of the other above-mentioned layers that display the same peculiar lithostratigraphic and geochemical features.

Concerning the most notable findings we provided on the C-22/Triflisco cluster, the oldest eruption of this cluster is Triflisco (92.8 ± 0.4 ka $^{40}Ar/^{39}Ar$ age, 93.7 ± 0.7 modelled age), whose material was mainly dispersed northwards and moderately east-southwards, as documented by its occurrence with notable thickness in Sulmona (POP1), Fucino (TF-10), Adriatic Sea (PRAD 2517), Monticchio (TM-23-11) and, as a thin layer, also in the Tyrrhenian Sea (DED-B and CET1 crypto-11) (Fig. 13b).

Triflisco was then followed by the ~0.5 ka younger eruption (93.2 ± 0.7 ka modelled age; Fig. 12 and Table 1) of the Triflisco-C-22 IEEs (San Prisco CSP-3/TM-23-8/-9/-10), likely mainly dispersed eastwards (San Gregorio Magno S14 and Tenaghi Philippon TP05–25.195) (Fig. 13b) and finally by the ~0.8 ka younger C-22 eruption (90.4 ± 1.6 ka $^{40}Ar/^{39}Ar$ age, 92.9 ± 0.8 ka modelled age), which was dispersed southwards, mainly in the Tyrrhenian Sea (Fig. 13b). Notably, according to the Bayesian age-depth model, this cluster of eruptions may have occurred in a shorter time span than those determined by $^{40}Ar/^{39}Ar$ dating, i.e., 0.8 ± 1.1 kyr versus 2.4 ± 1.6 kyr, which would implicate a high eruption frequency.

Our revised tephrochronology also allowed to provide the modelled ages of the other layers found in the DED 87-08 Tyrrhenian Sea core and correlated to tephra layers in the Monticchio record (e.g., DED-D, E, F, C-

26, DED-L, M, N; Fig. 12, Table 1). Beyond the uncertainties of the high-resolution modelled tephra ages, this study provides the first, statistically significant chronological data for several unknown and undated CF eruptions (Fig. 11 and Table 1), thus improving the general knowledge of the timing of the explosive activity for this caldera between ~90 ka and ~110 ka (Fig. 14). On a longer time-scale, the paucity of data and detailed investigations for the interval preceding Maddaloni (109 ka) and Taurano Ignimbrite (159 ka) currently prevent a meaningful assessment of the CF activity. Nevertheless, several indications from both distal (e.g., Wulf et al., 2012; Petrosino et al., 2019; Paterne et al., 2008; Monaco et al., 2022b) and proximal (De Vivo et al., 2001; Rolandi et al., 2003) records suggest that it could be conspicuous. A preliminary synthesis of the potential CF tephra occurring in these still poorly explored intervals, not specifically addressed in this study and that call for future investigations, is shown in Fig. 14.

6. Conclusions

During the last two decades, fundamental steps forward have been made to help better define the pre-CI volcanic history at Campi Flegrei, as summarised in this literature review of the volcanic activity at Campi Flegrei occurred at ~160 ka and from ~110 to ~90 ka. This dataset, combined with new investigations from mid-distal (Campanian Plain), distal (Tyrrhenian Sea) and ultra-distal (Lower Danube loess area) settings, allowed us to confirm some of the previous correlations (e.g., C-27 with X-5 and C-31 with X-6 eruption), but also to reappraise some of the previous attributions and refine both CF explosive history and Mediterranean tephrostratigraphy. Of great significance is the recognition of multiple eruptions (Triflisco-C-22 IEEs) within the brief interval of ~93-90 ka, even shorter according to the Bayesian age-depth model (~93.7-92.9 ka), whose deposits were previously undistinguished and correlated to an individual and widespread Mediterranean marker tephra.

Even though we are still far from an accurate knowledge of the volcanic history of the Campi Flegrei and dynamics of the eruptions at ~160 ka and between 110 ka and 90 ka, we were able to highlight the occurrence of at least 13 CF explosive eruptions during this period, 12 of which within the short time period of ~19 kyr, between 109 ka and ~90 ka. Thus, new potential eruptive events have been included in the history of the volcano. By combining new and literature $^{40}Ar/^{39}Ar$ ages we built a Bayesian age-depth model, providing statistically significant chronological constraints also for undated and undefined CF units, in order to reconstruct the explosive history and understate the temporal evolution of the early stage of CF caldera. Eventually, the new investigations allowed us to recognize several “tephra-like” layers in the DED 87-08 core that are not primary deposits but may have been generated by secondary processes linked both to CF and Ischia Island instabilities.

This work helps shed light on the still poorly known but significant early phase of the CF at ~160 ka and between ~110 ka and ~90, whose knowledge is essential to fully understand the magmatic and volcanic evolution of this complex caldera. In this regard, our work represents a further step toward a better reconstruction of the long-term history of the CF, setting the basis for modelling dispersion as well as eruptive parameters of some of the well-characterised early CF explosive eruptions. On the other hand, our review also highlighted a potential CF activity over the interval between 110 ka and 160 ka and preceding 160 ka, which, however, cannot be ascertained and reliably assessed because of the current paucity of data. Future investigations, aimed at filling this gap of fundamental knowledge, are thus in order.

CRediT authorship contribution statement

Giada Fernandez: Conceptualization, Methodology, Investigation, Data curation, Writing – original draft, Writing – review & editing, Visualization. **Biagio Giaccio:** Conceptualization, Resources, Data curation, Writing – review & editing, Visualization, Supervision, Project administration, Funding acquisition. **Antonio Costa:** Conceptualization, Writing – review & editing, Supervision. **Lorenzo Monaco:** Investigation, Data curation, Writing – review & editing. **Sébastien Nomade:** Methodology, Formal analysis, Resources, Writing – review & editing, Supervision. **Paul G. Albert:** Formal analysis, Investigation, Resources, Writing – review & editing. **Alison Pereira:** Formal analysis, Writing – review & editing. **Molly Flynn:** Investigation. **Niklas Leicher:** Investigation, Resources, Writing – review & editing. **Federico Lucchi:** Resources. **Paola Petrosino:** Resources. **Danilo M. Palladino:** Writing – review & editing. **Alfonsa Milia:** Resources, Writing – review & editing. **Donatella Domenica Insinga:** Resources, Writing – review & editing. **Sabine Wulf:** Writing – review & editing. **Rebecca Kearney:** Resources. **Daniel Veres:** Resources, Writing – review & editing. **Diana Jordanova:** Resources, Writing – review & editing. **Maria Luisa Putignano:** Resources. **Roberto Isaia:** Resources. **Gianluca Sottili:** Conceptualization, Writing – review & editing, Visualization, Supervision, Project administration, Funding acquisition.

Declaration of competing interest

The authors declare that they have no known competing financial interests or personal relationships that could have appeared to influence the work reported in this paper.

Data availability

I have shared the data for this paper in the Supplemental files.

Acknowledgements

Dr. M. Mannetta is thanked for aiding the sample preparation process for the EMPA analyses. Dr. E. Braschi and A. Orlando are thanked for providing technical assistance during the EMPA analyses at Florence University. Dr. S. Tamburrino is thanked for sampling and providing grain-size data from the KC01B marine core. This research was financially supported by the project “The onset of alkaline-potassium magmatism in central Italy: how, when and why?” (PI: G. S.), funded by "Sapienza" University of Rome (Year 2020; prot. RM120172B9B69EB0). Field activities and grain-size analyses were financially supported by “Sapienza” University of Rome. WDS tephra analysis was supported by the projects FUTURE (MUR, PRIN 2017; grant 20177TKBXZ_003, G. Zanchetta coordinator) and COMET (MUR, PRIN 2022; grant 2022MS9KWR, B. Giaccio coordinator) financed by the Italian Research Ministry. PGA contribution was supported by a UKRI Future Leaders Fellowship (MR/S035478/1).

Appendix A. Supplementary data

Supplementary data to this article can be found online at https://doi.org/10.1016/j.quascirev.2024.108623.

References

Albert, P.G., Hardiman, M., Keller, J., Tomlinson, E.L., Smith, V.C., Bourne, A.J., Wulf, S., Zanchetta, G., Sulpizio, R., Müller, U.C., Pross, J., Ottolini, L., Matthews, I. P., Blockley, S.P.E., Menzies, M.A., 2015. Revisiting the Y-3 tephrostratigraphic marker: a new diagnostic glass geochemistry, age estimate, and details on its climatostratigraphical context. Quat. Sci. Rev. 118, 105–121. https://doi.org/10.1016/j.quascirev.2014.04.002.

Albert, P.G., Giaccio, B., Isaia, R., Costa, A., Niespolo, E.M., Nomade, S., Pereira, A., Renne, P.R., Hinchliffe, A., Mark, D.F., Brown, R.J., Smith, V.C., 2019. Evidence for a large-magnitude eruption from Campi Flegrei caldera (Italy) at 29 ka. Geology 47, 595–599. https://doi.org/10.1130/G45805.1.

Amato, V., Aucelli, P.P.C., Cesarano, M., Filocamo, F., Leone, N., Petrosino, P., Rosskopf, C.M., Valente, E., Casciello, E., Giralt, S., Jicha, B.R., 2018. Geomorphic response to late Quaternary tectonics in the axial portion of the Southern Apennines (Italy): a case study from the Calore River valley. Earth Surf. Process. Landforms 43, 2463–2480. https://doi.org/10.1002/esp.4390.

Balbas, A., Koppers, A.A., Kent, D.V., Konrad, K., Clark, P.U., 2016. Identification of the short-lived Santa rosa geomagnetic excursion in lavas on floreana island (galapagos) by $^{40}Ar/^{39}Ar$ geochronology. Geology 44 (1), 359–362. https://doi.org/10.1130/G37569.

Balescu, S., Jordanova, D., Brisson, L.F., Hardy, F., Huot, S., Lamothe, M., 2020. Luminescence chronology of the northeastern Bulgarian loess-paleosol sequences (Viatovo and Kaolinovo). Quat. Int. 552, 15–24. https://doi.org/10.1016/j.quaint.2019.04.020.

Belkin, H.E., Rolandi, G., Jackson, J.C., Cannatelli, C., Doherty, A.L., Petrosino, P., De Vivo, B., 2016. Mineralogy and geochemistry of the older (> 40 ka) ignimbrites on the Campanian Plain, southern Italy. Journal of Volcanology and Geothermal Research 323, 1–18. https://doi.org/10.1016/j.jvolgeores.2016.05.002.

Blaauw, M., Christen, J.A., 2011. Flexible paleoclimate age-depth models using an autoregressive gamma process. Bayesian Analysis 6, 457–474. https://doi.org/10.1214/11-BA618.

Blott, S.J., Pye, K., 2001. GRADISTAT: a grain size distribution and statistics package for the analysis of unconsolidated sediments. Earth Surf. Process. Landforms 26, 1237–1248. https://doi.org/10.1002/esp.261.

Bourne, A.J., Albert, P.G., Matthews, I.P., Trincardi, F., Wulf, S., Asioli, A., Blockley, S.P.E., Keller, J., Lowe, J.J., 2015. Tephrochronology of core PRAD 1-2 from the Adriatic Sea: insights into Italian explosive volcanism for the period 200–80 ka. Quat. Sci. Rev. 116, 28–43. https://doi.org/10.1016/j.quascirev.2015.03.006.

Bourne, A.J., Lowe, J.J., Trincardi, F., Asioli, A., Blockley, S.P.E., Wulf, S., Matthews, I. P., Piva, A., Vigliotti, L., 2010. Distal tephra record for the last ca 105,000 years from core PRAD 1-2 in the central Adriatic Sea: implications for marine tephrostratigraphy. Quaternary Science Reviews 29, 3079–3094. https://doi.org/10.1016/j.quascirev.2010.07.021.

Caron, B., Sulpizio, R., Zanchetta, G., Siani, G., Santacroce, R., 2010. The late holocene to Pleistocene tephrostratigraphic record of Lake Ohrid (Albania). Compt. Rendus Geosci. 342, 453–466. https://doi.org/10.1016/j.crte.2010.03.007.

Chen, X.Y., Blockley, S.P., Fletcher, R., Zhang, S., Kim, J.H., Park, M.H., Chen, C., Yin, J., Xu, Y.G., 2022. Holocene tephrostratigraphy in the East Sea/Japan Sea: implications for eruptive history of Ulleungdo volcano and potential for hemispheric synchronization of sedimentary archives. J. Geophys. Res. Solid Earth 127, e2021JB023243. https://doi.org/10.1029/2021JB023243.

Costa, A., Folch, A., Macedonio, G., Giaccio, B., Isaia, R., Smith, V.C., 2012. Quantifying volcanic ash dispersal and impact of the Campanian Ignimbrite super-eruption. Geophys. Res. Lett. 39 (10) https://doi.org/10.1029/2012GL051605.

Cox, S.E., Hemming, S.R., Tootell, D., 2020. The Isotopx NGX and ATONA faraday amplifiers. Geochronology 2, 231–243. https://doi.org/10.5194/gchron-2-231-2020.

De Vivo, B., Rolandi, G., Gans, P.B., Calvert, A., Bohrson, W.A., Spera, F.J., Belkin, H.E., 2001. New constraints on the pyroclastic eruptive history of the Campanian volcanic Plain (Italy). Mineral. Petrol. 73, 47–65. https://doi.org/10.1007/s007100170010.

Deino, A.L., Orsi, G., de Vita, S., Piochi, M., 2004. The age of the Neapolitan Yellow Tuff caldera-forming eruption (Campi Flegrei caldera–Italy) assessed by $^{40}Ar/^{39}Ar$ dating method. J. Volcanol. Geoth. Res. 133, 157–170. https://doi.org/10.1016/S0377-0273(03)00396-2.

Di Vito, M.A., Isaia, R., Orsi, G., Southon, J.D., De Vita, S., d'Antonio, M., Pappalardo, L., Piochi, M., 1999. Volcanism and deformation since 12,000 years at the Campi Flegrei caldera (Italy). J. Volcanol. Geoth. Res. 91, 221–246. https://doi.org/10.1016/S0377-0273(99)00037-2.

Di Vito, M.A., Sulpizio, R., Zanchetta, G., D'Orazio, M., 2008. The late Pleistocene pyroclastic deposits of the Campanian Plain: new insights into the explosive activity of Neapolitan volcanoes. J. Volcanol. Geoth. Res. 177, 19–48. https://doi.org/10.1016/j.jvolgeores.2007.11.019.

Donato, P., Albert, P.G., Crocitti, M., De Rosa, R., Menzies, M.A., 2016. Tephra layers along the southern Tyrrhenian coast of Italy: links to the X-5 & X-6 using volcanic glass geochemistry. J. Volcanol. Geoth. Res. 317, 30–41. https://doi.org/10.1016/j.jvolgeores.2016.02.023.

Folk, R.L., 1966. A review of grain-size parameters. Sedimentology 6, 73–93. https://doi.org/10.1111/j.1365-3091.1966.tb01572.x.

Folk, R.L., Ward, W.C., 1957. Brazos River bar [Texas]; a study in the significance of grain size parameters. J. Sediment. Res. 27, 3–26. https://doi.org/10.1306/74D70646-2B21-11D7-8648000102C1865D.

Freundt, A., Schindlbeck-Belo, J.C., Kutterolf, S., Hopkins, J.L., 2023. Tephra layers in the marine environment: a review of properties and emplacement processes. Geological Society, London, Special Publications 520, 595–637. https://doi.org/10.1144/SP520-2021-50.

Giaccio, B., Nomade, S., Wulf, S., Isaia, R., Sottili, G., Cavuoto, G., Galli, P., Messina, P., Sposato, A., Sulpizio, R., Zanchetta, G., 2012. The late MIS 5 Mediterranean tephra markers: a reappraisal from peninsular Italy terrestrial records. Quat. Sci. Rev. 56, 31–45. https://doi.org/10.1016/j.quascirev.2012.09.009.

Giaccio, B., Hajdas, I., Isaia, R., Deino, A., Nomade, S., 2017a. High-precision 14C and 40Ar/39Ar dating of the Campanian Ignimbrite (Y-5) reconciles the time-scales of climatic-cultural processes at 40 ka. Sci. Rep. 7, 1–10. https://doi.org/10.1038/srep45940.

Giaccio, B., Niespolo, E.M., Pereira, A., Nomade, S., Renne, P.R., Albert, P.G., Arienzo, I., Regattieri, E., Wagner, B., Zanchetta, G., Gaeta, M., Galli, P., Mannella, G., Peronace, E., Sottili, G., Florindo, F., Leicher, N., Marra, F., Tomlinson, E.L., 2017b. First integrated tephrochronological record for the last~ 190 kyr from the Fucino Quaternary lacustrine succession, central Italy. Quat. Sci. Rev. 158, 211–234. https://doi.org/10.1016/j.quascirev.2017.01.004.

Giaccio, B., Leicher, N., Mannella, G., Monaco, L., Regattieri, E., Wagner, B., Zanchetta, G., Gaeta, M., Marra, F., Nomade, S., Palladino, D.M., Pereira, A., Scheidt, S., Sottili, G., Wonik, T., Wulf, S., Zeeden, C., Ariztegui, D., Cavinato, G.P., Dean, J.R., Tzedakis, P.C., 2019. Extending the tephra and palaeoenvironmental record of the Central Mediterranean back to 430 ka: a new core from Fucino Basin, central Italy. Quat. Sci. Rev. 225, 106003 https://doi.org/10.1016/j.quascirev.2019.106003.

Giraudi, C., Giaccio, B., 2017. Middle Pleistocene glaciations in the Apennines, Italy: new chronological data and preservation of the glacial record. Geological Society, London, Special Publications 433, 161–178. https://doi.org/10.1144/SP433.1.

Insinga, D.D., Tamburrino, S., Lirer, F., Vezzoli, L., Barra, M., De Lange, G.J., Tiepolo, M., Vallefuoco, M., Mazzola, S., Sprovieri, M., 2014. Tephrochronology of the astronomically-tuned KC01B deep-sea core, Ionian Sea: insights into the explosive activity of the Central Mediterranean area during the last 200 ka. Quat. Sci. Rev. 85, 63–84. https://doi.org/10.1016/j.quascirev.2013.11.019.

Iorio, M., Liddicoat, J., Budillon, F., Incoronato, A., Coe, R.S., Insinga, D.D., Cassata, W. S., Lubritto, C., Angelino, A., Tamburrino, S., 2014. Combined palaeomagnetic secular variation and petrophysical records to time-constrain geological and hazardous events: an example from the eastern Tyrrhenian Sea over the last 120 ka. Global Planet. Change 113, 91–109. https://doi.org/10.1016/j.gloplacha.2013.11.005.

Jochum, K.P., Stoll, B., Herwig, K., Willbold, M., Hofmann, A.W., Amini, M., Aarbug, S., Abouchami, W., Hellebrand, E., Mocek, B., Raczek, I., Stracke, A., Alard, O., Bouman, C., Becker, S., Dücking, M., Brätz, H., Klemd, R., de Bruin, D., Canil, D., Cornell, D., Hoog, C.-S., Dalpé, C., Danyushevsky, L., Eisenhauer, A., Gao, Y., Snow, J.E., Groschopf, N., Günther, D., Latkoczy, C., Guillong, M., Hauri, E.K., Höfer, H.E., Lahaye, Y., Horz, K., Jacob, D.E., Kasemann, S.A., Kent, A.J.R., Ludwig, T., Zack, T., Mason, P.R.D., Meixner, A., Rosner, M., Kisawa, K., Nash, P.B., Pfänder, J., Premo, W.R., Sun, W.D., Tiepolo, M., Vannucci, R., Vennemann, T., Wayne, D., Woodhead, J.D., 2006. MPI-DING reference glasses for in situ microanalysis: new reference values for element concentrations and isotope ratios. G-cubed 7. https://doi.org/10.1029/2005GC001060.

Jordan, N.J., Rotolo, S.G., Williams, R., Speranza, F., McIntosh, W.C., Branney, M.J., Scaillet, S., 2018. Explosive eruptive history of Pantelleria, Italy: repeated caldera collapse and ignimbrite emplacement at a peralkaline volcano. J. Volcanol. Geoth. Res. 349, 47–73. https://doi.org/10.1016/j.jvolgeores.2017.09.013.

Jordanova, D., Laag, C., Jordanova, N., Lagroix, F., Georgieva, B., Ishlyamski, D., Guyodo, Y., 2022. A detailed magnetic record of Pleistocene climate and distal ash dispersal during the last 800 kyrs-The Suhia Kladenetz quarry loess-paleosol sequence near Pleven (Bulgaria). Global Planet. Change 214, 103840. https://doi.org/10.1016/j.gloplacha.2022.103840.

Kallel, N., Duplessy, J.C., Labeyrie, L., Fontugne, M., Paterne, M., Montacer, M., 2000. Mediterranean pluvial periods and sapropel formation over the last 200 000 years. Palaeogeogr. Palaeoclimatol. Palaeoecol. 157, 45–58. https://doi.org/10.1016/S0031-0182(99)00149-2.

Keller, J., Ryan, W.B.F., Ninkovich, D., Altherr, R., 1978. Explosive volcanic activity in the Mediterranean over the past 200,000 yr as recorded in deep-sea sediments. Geol. Soc. Am. Bull. 89, 591–604. https://doi.org/10.1130/0016-7606(1978)89<591:EVAITM>2.0.CO;2.

Koppers, A.A., 2002. ArArCALC—software for $^{40}Ar/^{39}Ar$ age calculations. Comput. Geosci. 28, 605–619. https://doi.org/10.1016/S0098-3004(01)00095-4.

Kuehn, S.C., Froese, D.G., Shane, P.A., Participants, I.I., 2011. The INTAV intercomparison of electron-beam microanalysis of glass by tephrochronology laboratories: results and recommendations. Quat. Int. 246, 19–47. https://doi.org/10.1016/j.quaint.2011.08.022.

Le Maitre, R., Streckeisen, A., Zanettin, B., Le Bas, M., Bonin, B., Bateman, P., 2002. Igneous Rocks: A Classification and Glossary of Terms: Recommendations of the International Union of Geological Sciences Subcommission on the Systematics of Igneous Rocks, second ed. Cambridge University Press, Cambridge.

Lee, J.Y., Marti, K., Severinghaus, J.P., Kawamura, K., Yoo, H.S., Lee, J.B., Kim, J.S., 2006. A redetermination of the isotopic abundances of atmospheric Ar. Geochem. Cosmochim. Acta 70, 4507–4512. https://doi.org/10.1016/j.gca.2006.06.1563.

Leicher, N., Zanchetta, G., Sulpizio, R., Giaccio, B., Wagner, B., Nomade, S., Francke, A., Del Carlo, P., 2016. First tephrostratigraphic results of the DEEP site record from Lake Ohrid (Macedonia and Albania). Biogeosciences 13, 2151–2178. https://doi.org/10.5194/bg-13-2151-2016.

Leicher, N., Giaccio, B., Zanchetta, G., Sulpizio, R., Albert, P.G., Tomlinson, E.L., Lagos, M., Francke, A., Wagner, B., 2021. Lake Ohrid's tephrochronological dataset reveals 1.36 Ma of Mediterranean explosive volcanic activity. Scientific Data 8, 231. https://doi.org/10.1038/s41597-021-01013-7.

Leicher, N., Giaccio, B., Zanchetta, G., Wagner, B., Francke, A., Palladino, D.M., Sulpizio, R., Albert, P.G., Tomlinson, E.L., 2019. Central Mediterranean explosive volcanism and tephrochronology during the last 630 ka based on the sediment record from Lake Ohrid. Quat. Sci. Rev. 226, 106021 https://doi.org/10.1016/j.quascirev.2019.106021.

Lomax, J., Fuchs, M., Antoine, P., Rousseau, D.D., Lagroix, F., Hatté, C., Till, J.L., Debret, M., Moine, O., Taylor, S.N., Jordanova, D., 2019. A luminescence-based chronology for the Harletz loess sequence, Bulgaria. Boreas 48, 179–194. https://doi.org/10.1111/bor.12348.

Lowe, D.J., 2011. Tephrochronology and its application: a review. Quat. Geochronol. 6, 107–153. https://doi.org/10.1016/j.quageo.2010.08.003.

Lucchi, F., Keller, J., Tranne, C.A., 2013. Regional stratigraphic correlations across the Aeolian archipelago (southern Italy). Geological Society 37, 55–81. https://doi.org/10.1144/M37.6. London, Memoirs.

Ludwig, K.R., 2003. Isoplot 3.0a, a Geochronological Toolkit for Microsoft Excel, vol. 4. Berkeley Geochronology Center Special Publication.

Mahood, G.A., Hildreth, W., 1986. Geology of the peralkaline volcano at Pantelleria, strait of sicily. Bull. Volcanol. 48, 143–172. https://doi.org/10.1007/BF01046548.

Marani, M.P., Gamberi, F., 2004. Structural Framework of the Tyrrhenian Sea Unveiled by Seafloor Morphology, vol. 64. Memorie Descrittive della Carta Geologica d'Italia, 972108.

Marciano, R., Munno, R., Petrosino, P., Santangelo, N., Santo, A., Villa, I., 2008. Late quaternary tephra layers along the Cilento coastline (southern Italy). J. Volcanol. Geoth. Res. 177, 227–243. https://doi.org/10.1016/j.jvolgeores.2007.11.009.

Marianelli, P., Sbrana, A., 1998. Risultati di misure di standard di minerali e di vetri naturali in microanalisi a dispersione di energia. Atti Soc Tosc Sc Nat Resid Pisa, Mem, Serie A 105, 57–63.

Marti, A., Folch, A., Costa, A., Engwell, S., 2016. Reconstructing the plinian and co-ignimbrite sources of large volcanic eruptions: a novel approach for the Campanian Ignimbrite. Sci. Rep. 6, 21220 https://doi.org/10.1038/srep21220.

Martin-Puertas, C., Brauer, A., Wulf, S., Ott, F., Lauterbach, S., Dulski, P., 2014. Annual proxy data from Lago Grande di Monticchio (southern Italy) between 76 and 112 ka: new chronological constraints and insights on abrupt climatic oscillations. Clim. Past 10, 2099–2114. https://doi.org/10.5194/cp-10-2099-2014.

Massaro, S., Stocchi, M., Martínez Montesinos, B., Sandri, L., Selva, J., Sulpizio, R., Giaccio, B., Moscatelli, M., Peronace, E., Nocentini, M., Isaia, R., Luzòn, M.T., Dellino, P., Naso, G., Costa, A., 2023. Assessing long-term tephra fallout hazard in southern Italy from Neapolitan volcanoes. Nat. Hazards Earth Syst. Sci. 23, 2289–2311. https://doi.org/10.5194/nhess-23-2289-2023.

Milia, A., 2000. The Dohrn canyon: a response to the eustatic fall and tectonic uplift of the outer shelf along the eastern Tyrrhenian Sea margin, Italy. Geo Mar. Lett. 20, 101–108. https://doi.org/10.1007/s003670000044.

Milia, A., Torrente, M.M., 2007. The influence of paleogeographic setting and crustal subsidence on the architecture of ignimbrites in the Bay of Naples. Earth Planet Sci. Lett. 263, 192–206. https://doi.org/10.1016/j.epsl.2007.08.004.

Milia, A., Torrente, M.M., 2011. The possible role of extensional faults in localizing magmatic activity: a crustal model for the Campanian Volcanic Zone (eastern Tyrrhenian Sea, Italy). J. Geol. Soc. 168, 471–484. https://doi.org/10.1144/0016-76492010-121.

Monaco, L., Palladino, D.M., Albert, P.G., Arienzo, I., Conticelli, S., Di Vito, M., Fabbrizio, A., D'Antonio, M., Isaia, R., Manning, C.J., Nomade, S., Pereira, A., Petrosino, P., Sottili, G., Sulpizio, R., Zanchetta, G., Giaccio, B., 2022a. Linking the Mediterranean MIS 5 tephra markers to Campi Flegrei (southern Italy) 109–92 ka explosive activity and refining the chronology of MIS 5c-d millennial-scale climate variability. Global Planet. Change 211, 103785. https://doi.org/10.1016/j.gloplacha.2022.103785.

Monaco, L., Leicher, N., Palladino, D.M., Arienzo, I., Marra, F., Petrelli, M., Nomade, S., Pereira, A., Sottili, G., Conticelli, S., D'Antonio, M., Fabbrizio, A., Jicha, B.R., Mannella, G., Petrosino, P., Regattieri, E., Tzedakis, P.C., Wagner, B., Zanchetta, G., Giaccio, B., 2022b. The Fucino 250–170 ka tephra record: new insights on peri-Tyrrhenian explosive volcanism, central mediterranean tephrochronology, and timing of the MIS 8-6 climate variability. Quat. Sci. Rev. 296, 107797 https://doi.org/10.1016/j.quascirev.2022.107797.

Munno, R., Petrosino, P., 2007. The late Quaternary tephrostratigraphical record of the San Gregorio Magno basin (southern Italy). J. Quat. Sci. 22, 247–266. https://doi.org/10.1002/jqs.1025.

Natale, J., Camanni, G., Ferranti, L., Isaia, R., Sacchi, M., Spiess, V., Steinmann, L., Vitale, S., 2022b. Fault systems in the offshore sector of the Campi Flegrei caldera (southern Italy): Implications for nested caldera structure, resurgent dome, and volcano-tectonic evolution. Journal of Structural Geology 163, 104723. https://doi.org/10.1016/j.jsg.2022.104723.

Natale, J., Ferranti, L., Isaia, R., Marino, C., Sacchi, M., Spiess, V., Steinmann, L., Vitale, S., 2022a. Integrated on-land-offshore stratigraphy of the Campi Flegrei caldera: New insights into the volcano-tectonic evolution in the last 15 kyr. Basin Research 34, 855–882. https://doi.org/10.1111/bre.12643.

Newhall, C.G., Self, S., 1982. The volcanic explosivity index (VEI) an estimate of explosive magnitude for historical volcanism. J. Geophys. Res. 87, 1231–1238. https://doi.org/10.1029/JC087iC02p01231.

Niespolo, E.M., Rutte, D., Deino, A.L., Renne, P.R., 2017. Intercalibration and age of the Alder Creek sanidine $^{40}Ar/^{39}Ar$ standard. Quat. Geochronol. 39, 205–213. https://doi.org/10.1016/j.quageo.2016.09.004.

Paterne, M., Guichard, F., Labeyrie, J., 1988. Explosive activity of the South Italian volcanoes during the last 80,000 years as determined by marine tephrochronology. J. Volcanol. Geoth. Res. 34 (3–4), 153–172. https://doi.org/10.1016/0377-0273(88)90030-3.

Paterne, M., Guichard, F., Duplessy, J.C., Siani, G., Sulpizio, R., Labeyrie, J., 2008. A 90,000–200,000 yrs marine tephra record of Italian volcanic activity in the Central Mediterranean Sea. J. Volcanol. Geoth. Res. 177, 187–196. https://doi.org/10.1016/j.jvolgeores.2007.11.028.

Petrosino, P., Morabito, S., Jicha, B.R., Milia, A., Sprovieri, M., Tamburrino, S., 2016. Multidisciplinary tephrochronological correlation of marker events in the eastern Tyrrhenian Sea between 48 and 105 ka. J. Volcanol. Geoth. Res. 315, 79–99. https://doi.org/10.1016/j.jvolgeores.2016.02.001.

PsyTeachR Team, 2022. Open-source tutorials benefit the field. Nature Reviews Psychology 1, 312–313. https://doi.org/10.1038/s44159-022-00058-8.

Regattieri, E., Giaccio, B., Zanchetta, G., Drysdale, R.N., Galli, P., Nomade, S., Peronace, E., Wulf, S., 2015. Hydrological variability over the Apennines during the Early Last Glacial precession minimum, as revealed by a stable isotope record from Sulmona basin, Central Italy. J. Quat. Sci. 30, 19–31. https://doi.org/10.1002/jqs.2755.

Regattieri, E., Giaccio, B., Nomade, S., Francke, A., Vogel, H., Drysdale, R.N., Perchiazzi, N., Wagner, B., Gemelli, M., Mazzini, I., Boschi, C., Galli, P., Peronace, E., 2017. A last interglacial record of environmental changes from the Sulmona Basin (central Italy). Palaeogeogr. Palaeoclimatol. Palaeoecol. 472, 51–66. https://doi.org/10.1016/j.palaeo.2017.02.013.

Renne, P.R., Balco, G., Ludwig, K.R., Mundil, R., Min, K., 2011. Response to the comment by WH Schwarz et al. on "Joint determination of 40 K decay constants and $^{40}Ar^*/^{40}K$ for the Fish Canyon sanidine standard, and improved accuracy for $^{40}Ar/^{39}Ar$ geochronology". In: Renne, P.R., et al. (Eds.), Geochimica et Cosmochimica Acta, vol. 75, pp. 5097–5100. https://doi.org/10.1016/j.gca.2011.06.021, 2010.

Rolandi, G., Bellucci, F., Heizler, M.T., Belkin, H.E., De Vivo, B., 2003. Tectonic controls on the genesis of ignimbrites from the Campanian Volcanic Zone, southern Italy. Mineral. Petrol. 79, 3–31. https://doi.org/10.1007/s00710-003-0014-4.

Rotolo, S.G., Scaillet, S., La Felice, S., Vita-Scaillet, G., 2013. A revision of the structure and stratigraphy of pre-Green Tuff ignimbrites at Pantelleria (Strait of Sicily). J. Volcanol. Geoth. Res. 250, 61–74. https://doi.org/10.1016/j.jvolgeores.2012.10.009.

Rotolo, S.G., Scaillet, S., Speranza, F., White, J.C., Williams, R., Jordan, N.J., 2021. Volcanological evolution of Pantelleria island (strait of sicily) peralkaline volcano: a review. Compt. Rendus Geosci. 353, 111–132. https://doi.org/10.5802/crgeos.51.

Sammartini, M., Camerlenghi, A., Budillon, F., Insinga, D.D., Zgur, F., Conforti, A., Iorio, M., Romeo, R., Tonielli, R., 2019. Open-slope, translational submarine landslide in a tectonically active volcanic continental margin (Licosa submarine landslide, southern Tyrrhenian Sea). Geological Society, London, Special Publications 477, 133–150. https://doi.org/10.1144/SP477.34.

Satow, C., Tomlinson, E.L., Grant, K.M., Albert, P.G., Smith, V.C., Manning, C.J., Ottolini, L., Wulf, S., Rohling, E.J., Lowe, J.J., Blockey, S.P.E., Menzies, M.A., 2015. A new contribution to the late quaternary tephrostratigraphy of the mediterranean: Aegean Sea core LC21. Quat. Sci. Rev. 117, 96–112. https://doi.org/10.1016/j.quascirev.2015.04.005.

Silleni, A., Giordano, G., Isaia, R., Ort, M.H., 2020. The magnitude of the 39.8 ka Campanian Ignimbrite eruption, Italy: method, uncertainties and errors. Front. Earth Sci. 8, 543399 https://doi.org/10.3389/feart.2020.543399.

Smith, V.C., Isaia, R., Engwell, S.L., Albert, P.G., 2016. Tephra dispersal during the Campanian Ignimbrite (Italy) eruption: implications for ultra-distal ash transport during the large caldera-forming eruption. Bulletin of Volcanology 78, 1–15. https://doi.org/10.1007/s00445-016-1037-0.

Smith, V.C., Isaia, R., Pearce, N.J.G., 2011. Tephrostratigraphy and glass compositions of post-15 kyr Campi Flegrei eruptions: implications for eruption history and chronostratigraphic markers. Quat. Sci. Rev. 30, 3638–3660. https://doi.org/10.1016/j.quascirev.2011.07.012.

Smith, V.C., Costa, A., Aguirre-Díaz, G., Pedrazzi, D., Scifo, A., Plunkett, G., Poret, M., Tournigand, P.Y., Miles, D., Dee, M.W., McConnell, J.R., Sunyé-Puchol, I., Dàvila-Harris, P., Sigl, M., Pilcher, J.R., Chellman, N., Gutiérrez, E., 2020. The magnitude and impact of the 431 CE tierra blanca joven eruption of ilopango, El Salvador. In: Proceedings of the National Academy of Sciences, vol. 117, pp. 26061–26068. https://doi.org/10.1073/pnas.2003008117.

Speranza, F., Di Chiara, A., Rotolo, S.G., 2012. Correlation of welded ignimbrites on Pantelleria (Strait of Sicily) using paleomagnetism. Bull. Volcanol. 74, 341–357. https://doi.org/10.1007/s00445-011-0521-9.

Sulpizio, R., Bonasia, R., Dellino, P., Di Vito, M.A., La Volpe, L., Mele, D., Zanchetta, G., Sadori, L., 2008. Discriminating the long distance dispersal of fine ash from sustained columns or near ground ash clouds: the example of the Pomici di Avellino eruption (Somma-Vesuvius, Italy). J. Volcanol. Geoth. Res. 177, 263–276. https://doi.org/10.1016/j.jvolgeores.2007.11.012.

Sulpizio, R., Zanchetta, G., D'Orazio, M., Vogel, H., Wagner, B., 2010. Tephrostratigraphy and tephrochronology of lakes Ohrid and prespa, balkans. Biogeosciences 7, 3273–3288. https://doi.org/10.5194/bg-7-3273-2010.

Sulpizio, R., Folch, A., Costa, A., Scaini, C., Dellino, P., 2012. Hazard assessment of far-range volcanic ash dispersal from a violent Strombolian eruption at Somma-Vesuvius volcano, Naples, Italy: implications on civil aviation. Bull. Volcanol. 74, 2205–2218. https://doi.org/10.1007/s00445-012-0656-3.

Tomlinson, E.L., Arienzo, I., Civetta, L., Wulf, S., Smith, V.C., Hardiman, M., Lane, C.S., Carandente, A., Orsi, G., Rosi, M., Müller, W., Menzies, M.A., 2012. Geochemistry of the Phlegraean Fields (Italy) proximal sources for major Mediterranean tephras: implications for the dispersal of Plinian and co-ignimbritic components of explosive eruptions. Geochem. Cosmochim. Acta 93, 102–128. https://doi.org/10.1016/j.gca.2012.05.043.

Tomlinson, E.L., Albert, P.G., Wulf, S., Brown, R.J., Smith, V.C., Keller, J., Orsi, G., Bourne, A.J., Menzies, M.A., 2014. Age and geochemistry of tephra layers from Ischia, Italy: constraints from proximal-distal correlations with Lago Grande di Monticchio. J. Volcanol. Geoth. Res. 287, 22–39. https://doi.org/10.1016/j.jvolgeores.2014.09.006.

Tomlinson, E.L., Albert, P.G., Menzies, M.A., 2022. Tephrochronology and geochemistry of tephra from the Campi Flegrei volcanic field, Italy. In: Campi Flegrei. Springer, Berlin, Heidelberg, pp. 151–174. https://doi.org/10.1007/978-3-642-37060-1_5.

Torrente, M.M., Milia, A., Bellucci, F., Rolandi, G., 2010. Extensional tectonics in the Campania Volcanic Zone (eastern Tyrrhenian Sea, Italy): new insights into the relationship between faulting and ignimbrite eruptions. Italian Journal of Geosciences 129, 297–315. https://doi.org/10.3301/IJG.2010.07.

Vakhrameeva, P., Koutsodendris, A., Wulf, S., Portnyagin, M., Appelt, O., Ludwig, T., Trieloff, M., Pross, J., 2021. Land-sea correlations in the Eastern Mediterranean region over the past c. 800 kyr based on macro-and cryptotephras from ODP Site 964 (Ionian Basin). Quat. Sci. Rev. 255, 106811 https://doi.org/10.1016/j.quascirev.2021.106811.

Vineberg, S.O., Isaia, R., Albert, P.G., Brown, R.J., Smith, V.C., 2023. Insights into the explosive eruption history of Campanian volcanoes prior to the Campanian Ignimbrite eruption. J. Volcanol. Geoth. Res. 107915 https://doi.org/10.1016/j.jvolgeores.2023.107915.

Vitale, S., Isaia, R., 2014. Fractures and faults in volcanic rocks (Campi Flegrei, southern Italy): insight into volcano-tectonic processes. International Journal of Earth Sciences 103, 801–819. https://doi.org/10.1007/s00531-013-0979-0.

Vogel, H., Zanchetta, G., Sulpizio, R., Wagner, B., Nowaczyk, N., 2010. A tephrostratigraphic record for the last glacial–interglacial cycle from Lake Ohrid, Albania and Macedonia. J. Quat. Sci.: Published for the Quaternary Research Association 25, 320–338. https://doi.org/10.1002/jqs.1311.

Wulf, S., Kraml, M., Brauer, A., Keller, J., Negendank, J.F., 2004. Tephrochronology of the 100 ka lacustrine sediment record of Lago Grande di Monticchio (southern Italy). Quat. Int. 122, 7–30. https://doi.org/10.1016/j.quaint.2004.01.028.

Wulf, S., Brauer, A., Mingram, J., Zolitschka, B., Negendank, J.F., 2006. Distal tephras in the sediments of Monticchio maar lakes. *La geologia del monte Vulture*. Consiglio Nazionale delle Ricerche, pp. 105–122.

Wulf, S., Kraml, M., Keller, J., 2008. Towards a detailed distal tephrostratigraphy in the Central Mediterranean: the last 20,000 yrs record of Lago Grande di Monticchio. J. Volcanol. Geoth. Res. 177, 118–132. https://doi.org/10.1016/j.jvolgeores.2007.10.009.

Wulf, S., Keller, J., Paterne, M., Mingram, J., Lauterbach, S., Opitz, S., Sottili, G., Giaccio, B., Albert, P.G., Satow, C., Tomlinson, E.L., Viccaro, M., Brauer, A., 2012. The 100–133 ka record of Italian explosive volcanism and revised tephrochronology of Lago Grande di Monticchio. Quat. Sci. Rev. 58, 104–123. https://doi.org/10.1016/j.quascirev.2012.10.020.

Wulf, S., Hardiman, M.J., Staff, R.A., Koutsodendris, A., Appelt, O., Blockley, S.P., Lowe, J.J., Manning, C.J., Ottolini, L., Schmitt, A.K., Smith, V.C., Tomlinson, E.L., Vakhrameeva, P., Knipping, M., Kotthoff, U., Milner, A.M., Müller, U.C., Christanis, K., Kalaitzidis, S., Tzedakis, P.C., Schmiedl, G., Pross, J., 2018. The marine isotope stage 1–5 cryptotephra record of Tenaghi Philippon, Greece: towards a detailed tephrostratigraphic framework for the Eastern Mediterranean region. Quat. Sci. Rev. 186, 236–262. https://doi.org/10.1016/j.quascirev.2018.03.011.

Zanchetta, G., Sulpizio, R., Giaccio, B., Siani, G., Paterne, M., Wulf, S., D'Orazio, M., 2008. The Y-3 tephra: a Last Glacial stratigraphic marker for the central Mediterranean basin. J. Volcanol. Geoth. Res. 177, 145–154. https://doi.org/10.1016/j.jvolgeores.2007.08.017.

Zanchetta, G., Giaccio, B., Bini, M., Sarti, L., 2018. Tephrostratigraphy of Grotta del Cavallo, Southern Italy: insights on the chronology of Middle to Upper Palaeolithic transition in the Mediterranean. Quat. Sci. Rev. 182, 65–77. https://doi.org/10.1016/j.quascirev.2017.12.014.

Petrosino, P., Arienzo, I., Mazzeo, F. C., Natale, J., Petrelli, M., Milia, A., Perugini, D., D' Antonio, M., 2019. The San Gregorio Magno lacustrine basin (Campania, southern Italy): improved characterization of the tephrostratigraphic markers based on trace elements and isotopic data. Journal of Quaternary Science, 34, 393-404. https://doi.org/10.1002/jqs.3107.